Article

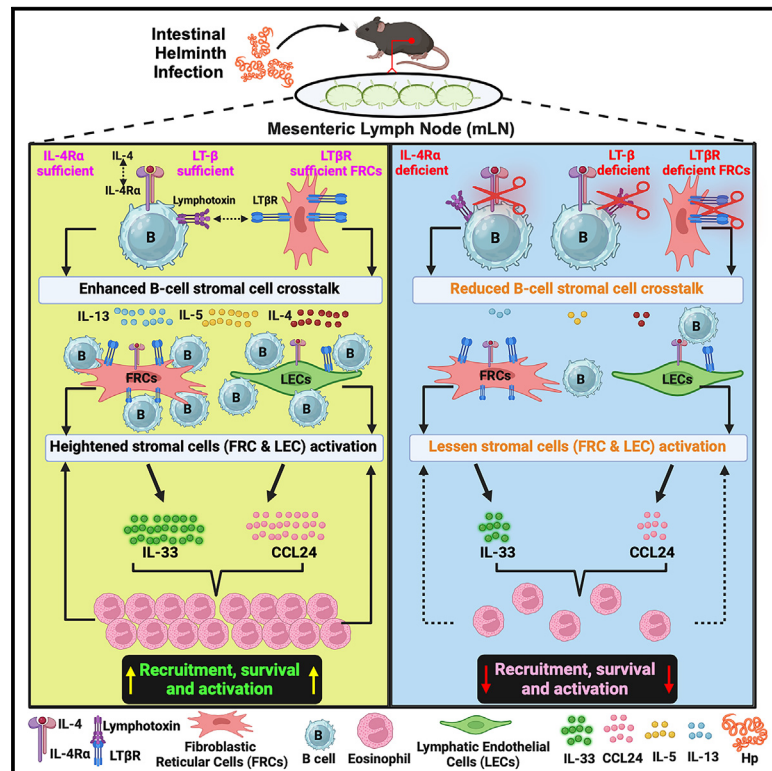# Stromal cell and B cell dialogue potentiates IL-33-enriched lymphoid niches to support eosinophil recruitment and function during type 2 immunity

Graphical abstract

Authors

Emily Bessell, Rachel E. Finlay,
Louisa K. James, ..., Philippe Krebs,
Matthew R. Hepworth, Lalit Kumar Dubey

Correspondence

lalit.dubey@qmul.ac.uk

In brief

Bessell et al. decode the mechanism behind recruitment, localization, survival, and activation of eosinophils within the mesenteric lymph node. They identify signals provided by B cells, fibroblastic reticular cells, and lymphatic endothelial cells, which regulate eosinophil association to distinct lymphoid niches, underscoring their role in type 2 immunity.

Highlights

- Helminth infection drives eosinophil recruitment and IFR localization within mLNs

- B cell-intrinsic IL-4Rα drives CCL24 expression in LECs, thus attracting eosinophils

- B cell-FRC dialogue via lymphotoxin-LTβR signaling yields IFR IL-33 during mLN eosinophilia

- Eosinophil synergism with FRCs and LECs enhances IL-33, CCL24, and type 2 immunity

CellPress

Article

Stromal cell and B cell dialogue potentiates IL-33-enriched lymphoid niches to support eosinophil recruitment and function during type 2 immunity

Emily Bessell,[1,4,7,8] Rachel E. Finlay,[2] Louisa K. James,[3] Burkhard Ludewig,[5] Nicola L. Harris,[6] Philippe Krebs,[4] Matthew R. Hepworth,[2] and Lalit Kumar Dubey[1,4,9,*]

[1]William Harvey Research Institute (WHRI), Barts & The London School of Medicine & Dentistry, Queen Mary University of London (QMUL), London, UK
[2]Division of Immunology, Immunity to Infection and Respiratory Medicine, Faculty of Biology, Medicine and Health, Lydia Becker Institute of Immunology and Inflammation, The University of Manchester, Manchester, UK
[3]Centre for Immunobiology, Blizard Institute, Queen Mary University of London, London, UK
[4]Institute of Tissue Medicine and Pathology, University of Bern, Bern, Switzerland
[5]Institute of Immunobiology, Kantonsspital St. Gallen, St. Gallen, Switzerland
[6]Department of Immunology and Pathology, Central Clinical School, Monash University, The Alfred Centre, Melbourne, VIC, Australia
[7]Institute of Parasitology, Vetsuisse Faculty, University of Bern, Bern, Switzerland
[8]Graduate School for Cellular and Biomedical Sciences, University of Bern, Bern, Switzerland
[9]Lead contact
*Correspondence: lalit.dubey@qmul.ac.uk
https://doi.org/10.1016/j.celrep.2024.114620

SUMMARY

Eosinophils are involved in host protection against multicellular organisms. However, their recruitment to the mesenteric lymph node (mLN) during type 2 immunity is understudied. Our results demonstrate that eosinophil association with lymphoid stromal niches constructed by fibroblastic reticular cells (FRCs) and lymphatic endothelial cells is diminished in mice selectively lacking interleukin (IL)-4Rα or lymphotoxin-β (LTβ) expression on B cells. Furthermore, eosinophil survival, activation, and enhanced *Il1rl1* receptor expression are driven by stromal cell and B cell dialogue. The ligation of lymphotoxin-β receptor (LTβR) on FRCs improves eosinophil survival and significantly augments IL-33 expression and eosinophil homing to the mLN, thus confirming the significance of lymphotoxin signaling for granulocyte recruitment. Eosinophil-deficient ΔdblGATA-1 mice show diminished mLN expansion, reduced interfollicular region (IFR) alarmin expression, and delayed helminth clearance, elucidating their importance in type 2 immunity. These findings provide insight into dialogue between stromal cells and B cells, which govern mLN eosinophilia, and the relevance of these mechanisms during type 2 immunity.

INTRODUCTION

Lymph nodes (LNs) are highly organized structures essential for eliciting the adaptive immune response by facilitating immune cell interactions. The non-hematopoietic portion of LNs consists of fibroblastic and endothelial stromal cells, which regulate and support immune cell migration and interaction within the LN.[1] Various stromal subtypes including fibroblastic reticular cells (FRCs), lymphatic endothelial cells (LECs), and follicular dendritic cells (FDCs) have been implicated in regulating the recruitment, migration, and localization of B cells, T cells, and dendritic cells (DCs) within the LN, which fosters close interactions between immune cells and facilitates the adaptive immune response.[2–4] The recruitment of lymphocytes and DCs to the LN requires CCR7 expression and is mainly driven by CCL19, CCL21, and CXCL13 produced by FRC subsets.[5] In contrast, emerging evidence suggests that granulocytes home to the LN

in a CCR7-independent manner to support lymphocyte function.[6,7] However, the association of lymphoid stromal cell subsets with granulocytes, such as eosinophils and their recruitment to distinct lymphoid niches during homeostasis and/or inflammation, is understudied.

Eosinophils are effector cells that mainly reside in the gastrointestinal tract and play a major role in homeostasis as well as in settings of type 2 immunity and inflammation, including helminth infections and allergy.[8–10] Eosinophils are terminally differentiated cells that originate in the bone marrow from granulocyte/macrophage progenitors and are present at low levels in the blood and mucosal surfaces under homeostatic conditions, such as the intestinal lamina propria and lungs. They accumulate in larger numbers in inflamed or infected tissues via a type 2 cytokine-mediated axis,[11] and not only amplify the type 2 response by secreting cytokines interleukin-4 (IL-4), IL-5, and IL-13[12,13] but cause extensive tissue damage during worm

expulsion due to degranulation; as a result, eosinophils are considered to be final stage effector cells. Alongside their effector functions, studies have shown that eosinophils have a major role in supporting the lymphoid adaptive immune response via B cell priming and survival,[14] antibody class switching, and maintaining gut homeostasis.[15,16]

B cell follicle formation and B cell survival are commonly associated with lymphoid stromal cells,[17] and previous studies have shown that following infection with the gastrointestinal helminth *Heligmosomoides polygyrus* (*Hp*), gut homeostasis is perturbed.[18] The anti-helminth type 2 response within the draining mesenteric lymph node (mLN) is characterized by an accumulation of T helper 2 (Th2) CD4$^+$ T cells, B cell follicle expansion, and extrafollicular B cell accumulation, which is supported by stromal subset expansion, proliferation, and remodeling at the interfollicular region (IFR).[17,19] FRC crosstalk with B cells governs the overall lymphoid stromal expansion and chemokine secretion to support strategic immune cell positioning, yet the role of B cell-stromal crosstalk in driving the recruitment of eosinophils into the mLN is poorly understood.

We and others have previously shown that following infection with *Hp*, IL-4, IL-5, and IL-13 were significantly increased in the mLN.[20,21] IL-4, IL-5, and IL-13, secreted from Th2 cells and group 2 innate lymphoid cells (ILC2s), activate eosinophils and drive eosinophilia[22] in infected or inflamed tissues by inducing the secretion of eosinophil-specific chemokines eotaxin-1 (CCL11), eotaxin-2 (CCL24), eotaxin-3 (CCL26), and RANTES (CCL5) from epithelial cells, macrophages, mononuclear cells, and fibroblasts.[9,23] However, the contribution of chemokine-induced eosinophil recruitment into lymphoid niches is largely unexplored, and little is known about the cellular source within the lymphoid niches that provide these eosinophil chemoattractants and survival signals.

Given the central role of stromal cells and B cells during the anti-helminth response[17,19] and the overlapping role of eosinophils in type 2 immunity and maintenance of B cell function, we asked what role B cells and stromal cells might play in eosinophil recruitment to the mLN and how this might support humoral immunity against helminth infection. Here, we found that during *Hp* infection eosinophils are recruited to the mLN in an IL-4 receptor α-chain (IL-4Rα)-dependent manner. Our results highlight a novel role of IL-4Rα signaling, which drives lymphotoxin expression on B cells during helminth infection. This is important for B cell-stromal crosstalk via lymphotoxin-β receptor (LTβR) ligation leading to chemoattractant and alarmin secretion by stromal cells that guides the recruitment, accumulation, and survival of eosinophils within the mLN. Eosinophils in turn can support the ongoing response in a synergistic manner as well as regulate the anti-helminth response, highlighting their unappreciated role in modulating the type 2 immune response.

RESULTS

Mesenteric lymph node eosinophilia requires IL-4Rα during helminth infection

Hp is a natural murine gastrointestinal helminth and serves as an excellent tool for studying type 2 immunity and as a model of chronic human helminth infection.[20] Helminth infection induces

eosinophilia in infected tissues; however, the mechanism behind the presence of eosinophils in secondary lymphoid organs, such as the mLN, is understudied. To evaluate mLN eosinophilia, we infected C57BL/6J mice with *Hp* and harvested the mLN from naive and infected mice. Using flow cytometry, we identified CD45$^+$CD3$^-$CD19$^-$CD11c$^-$FcεRI$^-$Ly6G$^-$CD11b$^+$Siglec-F$^+$ cells as eosinophils (Figure S1A), which were significantly increased within the mLN over the time course of infection (Figures 1A, 1B, and S1B). Both the percentage and absolute number of eosinophils within the mLN were significantly higher at 12 and 21 days post infection (dpi) compared to naive mice (Figures 1A and 1B). During *Hp* infection, a strong Th2 response is generated within the mLN, but not in Peyer's patches, and is characterized by high levels of IL-4, IL-5, and IL-13.[21] As both IL-4 and IL-13 signal through IL-4Rα, which is key to anti-helminth immunity,[20] we utilized IL-4Rα$^{-/-}$ as well as mice in which IL-13 had been deleted by a reporter allele insertion (IL-13$^{gfp/gfp}$ mice) to assess the role of these cytokine signaling pathways in mediating mLN eosinophilia. Following *Hp* infection, the entire chain of mLN was harvested from naive and infected wild-type (WT), IL-4Rα$^{-/-}$, and IL-13$^{gfp/gfp}$ mice and analyzed using flow cytometry. We observed a significant increase in the total weight and cellularity of the mLN post infection in WT but not in IL-4Rα$^{-/-}$ mice (Figures S1C and S1D), with the marked increase in eosinophil numbers seen in the infected WT mice ablated in infected IL-4Rα$^{-/-}$ mice (Figures 1C–1F). However, depletion of IL-13 alone (IL-13$^{gfp/gfp}$) was not sufficient to completely reduce the number of eosinophils following infection, suggesting that IL-13 signaling is dispensable for the recruitment of eosinophils into the mLN (Figures 1G and 1H). As eosinophilia into infected tissues is IL-5 dependent, we also analyzed the number of eosinophils in the mLNs of infected mice where IL-5 had been knocked down by inserting a reporter allele into the IL-5 locus (IL-5$^{R5/R5}$ mice; referred to as Red5/R5) and found that these mice had a significant reduction of eosinophils after *Hp* infection (Figures 1I and 1J), confirming that IL-5 also plays a role in eosinophilia into the mLN, as expected.[22]

As the spatial organization of the T cell and B cell zones following *Hp* infection is mediated by IL-4 signaling via IL-4Rα,[19] we considered the possibility that the lack of eosinophilia in IL-4Rα$^{-/-}$ mice may be a result of differential stromal remodeling.[17] To investigate this in detail, we conducted high-resolution multiplex imaging of WT and IL-4Rα$^{-/-}$ mLNs after *Hp* infection. These imaging studies revealed that WT infected mice had an increased accumulation of Siglec-F$^+$ eosinophils in the cortical and FRC-rich paracortical regions compared to naive mice (Figures S1E and S1F). Interestingly, in IL-4Rα$^{-/-}$ mice there were few Siglec-F$^+$ cells in the paracortical T cell zone (Figures S1G and S1H), with some accumulation of eosinophils in the medullary region. Collectively, these observations indicated that Siglec-F$^+$ eosinophils are recruited to and localize in distinct regions of mLN following helminth infection in an IL-4Rα-dependent manner. Therefore, IL-4Rα appears to regulate both the migration and localization of eosinophils within the mLN.

Next, we used multiplex imaging to extend these observations by taking advantage of the fact that *Hp* infection induces stromal remodeling and recruits immune cells to immune interactive sites
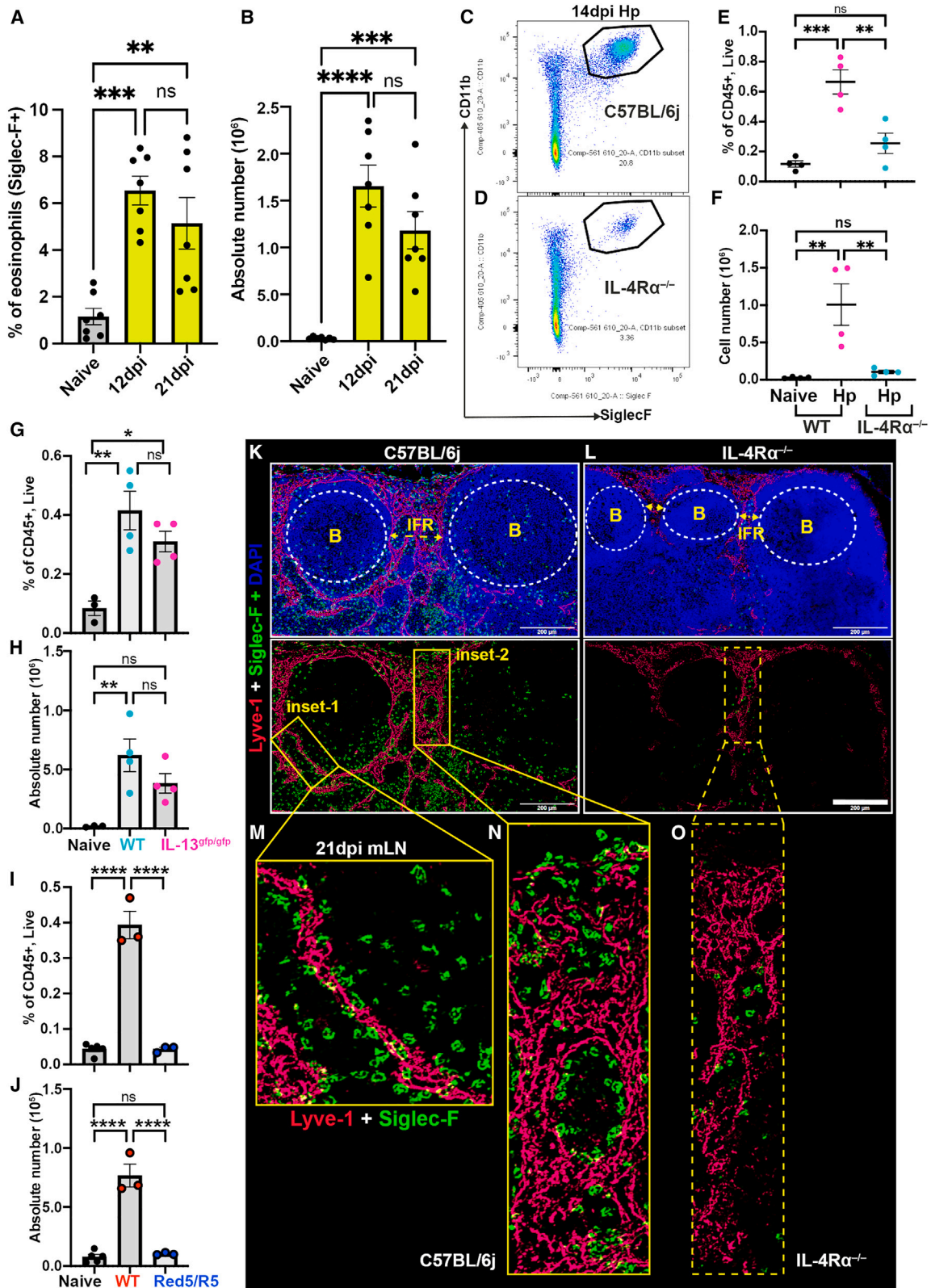
(legend on next page)

such as the T/B border and IFR.[19] Harvested mLNs from WT and IL-4R$\alpha^{-/-}$ mice at 0 (naive) and 21 dpi were stained for LECs (Lyve1^{+}) and eosinophils (Siglec-F[+]). LECs are key players in lymphocyte migration and, during *Hp* infection, expand throughout the LN cortical/IFR to support B cell follicle formation and T cell-DC interaction.[24] Lyve1 staining was performed to define and identify cortical, medullary, and paracortical segregation. In WT mice, eosinophils were recruited to the paracortical side of the T/B region (Figure 1K, inset 1) and the IFR (Figure 1K, inset 2) at 21 dpi, whereas in IL-4R$\alpha^{-/-}$ mice, fewer eosinophils were recruited to the IFR and/or the T/B border (Figures 1L and 1O). The naive mLN from both WT and IL-4R$\alpha^{-/-}$ mice showed no sign of eosinophilia (Figures S2A and S2B). This suggested that IL-4Rα supported the migration and localization of eosinophils into mLN immune interactive sites. High-resolution images of 21-dpi mLN from WT and IL-4R$\alpha^{-/-}$ mice showed a close association of lymphatic vessels and follicular B cell clusters alongside eosinophils (Figures 1M, 1N, and S2C), suggesting that eosinophils access the cortical lymphatic sinuses, which are known to serve as egress sites for immune cells in close association with the B cell follicle[25] and potentially support B cell function by providing survival factors and supporting antibody isotype class switching.[14,26] To further confirm eosinophil association with stromal cells, 21-dpi mLN from WT and IL-4R$\alpha^{-/-}$ mice were subjected to deep tissue imaging. Staining of vibratome sections further confirmed the enhanced eosinophilia in WT mice compared to IL-4R$\alpha^{-/-}$ mice, confirming the 2D histological findings (Videos S1 and S2). The observed close association of eosinophils with both FRCs and LECs suggests a potential role of stromal cells in mLN eosinophilia. Collectively, these observations highlight the previously unknown association of eosinophils with lymphoid stromal cells and suggest that IL-4Rα is key to their localization in distinct immunological niches within the mLN.

Non-hematopoietic stromal cells provide chemoattractants to support paracortical and interfollicular accumulation of eosinophils

Given the increase of eosinophils in the mLN post infection, translocation to distinct lymphoid niches, and association with stromal cells (Figures 1 and S1), we speculated that chemokine signals may arise from the mLN stroma to support eosinophil recruitment in an IL-4Rα-dependent manner. To evaluate this hypothesis, the total CD45^{-} stromal cells from naive and infected WT and IL-4R$\alpha^{-/-}$ mice were isolated for gene-expression analysis. The three key murine eosinophil chemoattractants, CCL5, CCL11, and CCL24, were evaluated for their relative expression in stromal fraction. All three genes were expressed by the CD45^{-} stromal fractions (Figures 2A–2C). A strong upregulation of *Ccl24* was observed during the early phase of infection in WT mice in an IL-4Rα-dependent manner, which remained elevated at later time points (Figure 2C), whereas an increase in *Ccl11* was observed during the later phase of infection, i.e., 12 dpi (Figure 2B). Interestingly, analysis of the key stromal subsets using the RNA-sequencing database Immgen.org confirmed the differential expression of eosinophil chemoattractants by the key stromal subsets found in secondary lymphoid organs (Figure 2D). All subsets express some CCL5, while FRCs had the highest expression of *Ccl11* and LECs expressed the most *Ccl24*. As CCL24 is a ligand for CCR3, highly expressed on eosinophils, and we saw enhanced *Ccl24* expression in the stromal fraction post infection, we further validated these findings using immunofluorescence microscopy with naive and infected mice mLN cryosections. mLN sections were stained with Lyve1, podoplanin (Pdpn), and CCL24. Interestingly, there was little to no detectable expression of CCL24 in naive mLN (Figure 2E). However, post *Hp* infection at 12 and 21 dpi, a significant increase in CCL24 expression was observed (Figures 2F and 2G). Closer analysis revealed that Lyve1^{+} LECs and not Lyve-1^{-}Pdpn[+] FRCs were the main source of CCL24 post infection (Figures 2F and 2G). To further corroborate these findings, we performed stromal cell isolation followed by stimulation with IL-4 *in vitro*. IL-4 stimulation of lymphoid stromal cells resulted in enhanced *Ccl24* expression, which was neutralized in the presence of an IL-4 neutralizing antibody (Figure S2D). These data suggested that the lymphatic endothelium is the principal cellular source of CCL24 during infection and provides an explanation for the preferential localization of eosinophils in proximity to the lymphatic vessels. Overall, these findings highlight the role of IL-4Rα-driven chemoattractant expression by stromal subsets within the mLN, which in turn regulates eosinophil recruitment and localization to distinct niches.

Figure 1. mLN eosinophilia and their interfollicular accumulation requires IL-4Rα

C57BL/6J (WT) mice were infected with *Hp*, and the entire chain of the mesenteric lymph node (mLN) was collected at 0 (naive), 12, and 21 dpi and analyzed by flow cytometry.

(A and B) (A) Percentage and (B) total number of CD11b^{+}Siglec-F^{+} eosinophils within the mLN. Data are pooled from two different independent experiments. Data represent mean ± SEM with $n \geq$ 3–4 mice per group.

(C and D) Pseudocolor dot plots showing eosinophils within the mLN of (C) WT and (D) IL-4Ra knockout (IL-4R$\alpha^{-/-}$) mice post *Hp* infection.

(E and F) (E) Percentage of eosinophils gated on CD45^{+} live cells and (F) absolute number of Siglec-F^{+} eosinophils within the mLN of WT and IL-4R$\alpha^{-/-}$ mice. IL-13[gfp/gfp] and IL-5[Red/R5] mice were infected with *Hp*, and the entire chain of the mLN was collected at 0 (naive) and 21 dpi and analyzed by flow cytometry.

(G–J) (G) Percentage and (H) absolute number of CD45^{+}CD11b^{+}Siglec-F^{+} cells in IL-13[gfp/gfp] mice, and (I) percentage and (J) absolute number of CD45^{+}CD11b^{+}Siglec-F^{+} cells in IL-5[Red/R5] mice. Data represent mean ± SEM and are representative of two independent experiments, with $n \geq$ 3–4 mice per group.

(K–O) WT and IL-4R$\alpha^{-/-}$ mice were infected with *Hp*, and the mLN was collected at 21 dpi. mLN cryosections showing combined staining for DAPI (blue), eosinophils (Siglec-F[+], green), and lymphatic endothelial cells (Lyve1^{+}, red) cells in (K) WT and (L) IL-4R$\alpha^{-/-}$ mice post *Hp* infection. The yellow inset-1 and inset-2 highlight the eosinophil accumulation at the paracortical region, T/B border, and interfollicular region (IFR), respectively. Eosinophil accumulation at the (M) paracortical and T/B border and (N) IFR in WT mice and (O) IFR in IL-4R$\alpha^{-/-}$ mice. Images are representative of $\geq$5 different experiments with $n \geq$ 2–3 mice/group/time point. Scale bar, 200 μm.

ns, not significant; *$p < 0.05$, **$p < 0.01$, ***$p < 0.001$, ****$p < 0.0001$ (ANOVA, Bonferroni's multiple comparison test).
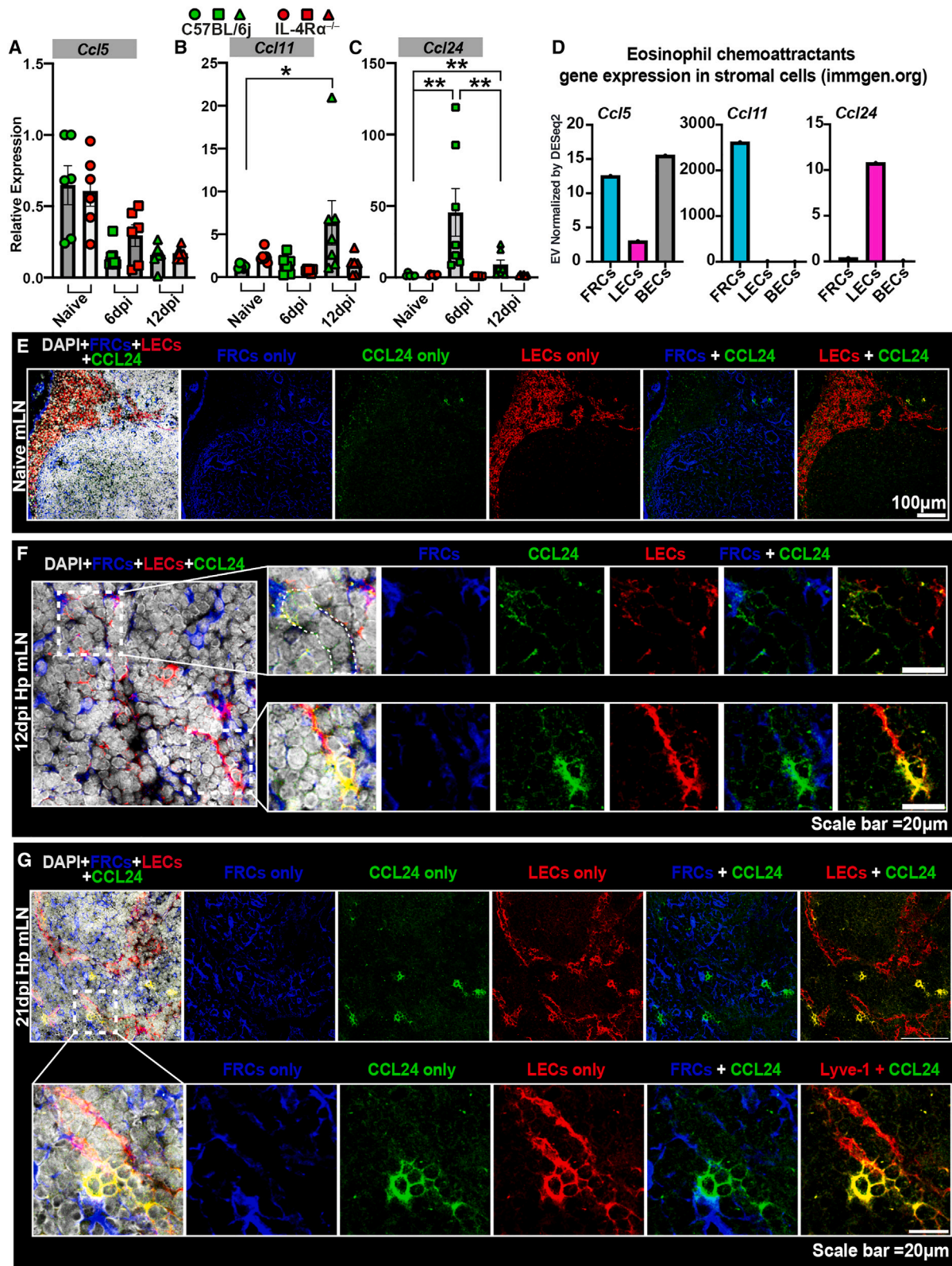
IL-4Rα governs both the cortical and cortical-medullary association of eosinophils with extrafollicular plasma cells

Following the observation that eosinophils localize within close vicinity of B cell follicles and lymphatics, we hypothesized that they would also be closely associated with mLN extrafollicular B cells and plasma cells. mLN sections from naive and infected WT and IL-4Rα$^{-/-}$ mice were analyzed immunohistochemically to confirm the localization of CD138$^+$ plasmablasts/plasma cells with the lymphatic sinuses present at cortical area and cortical-medullary junction.[27] Immunohistochemical staining of mLN serial sections showed that following infection there is an enhanced extrafollicular B cell response, whereas infected IL-4Rα$^{-/-}$ mice failed to mount such a response (Figures S3A and S3B). We observed that in the cortical-medullary and paracortical regions of the mLN in WT naive mice, there was little to no presence of eosinophils (Siglec-F$^+$) and plasmablasts/plasma cells (CD138$^+$) (Figure 3A, insets I and ii). Additionally, in the paracortical region, we observed no lymphatics (Lyve1$^+$), which correlated with the lack of eosinophils and plasma cells in this region. Comparatively, in the WT 21-dpi mice we observed a significant increase in both eosinophils and plasma cells in the cortical-medullary and paracortical regions (Figure 3B, insets iii and iv), a feature not evident in mice lacking IL-4Rα (Figure 3C, insets v and vi). Quantification of immunofluorescence images highlighting the area occupied by plasma cells and eosinophils complemented the immunohistochemical staining, showing that eosinophils and plasma cells co-existed within the mLN (Figures 3D and 3E). Additionally, quantitative analysis by flow cytometry highlighted that expansion of the CD138$^+$ plasma cell population following *Hp* infection is IL-4Rα dependent, with a significant reduction in plasma cell numbers in IL-4Rα$^{-/-}$ mice at 12 and 21 dpi compared to WT mice (Figures 3F and 3G). These data suggest that following helminth infection, IL-4Rα-driven expansion of the lymphatic network may support eosinophil and plasma cell co-localization in the cortical area and cortical-medullary junction as well as in the paracortical regions, which has the potential to support the extrafollicular B cell response, the key to anti-helminth antibody production.[17,28,29]

IL-4Rα deficiency in non-hematopoietic cells is dispensable to mLN eosinophilia

We next investigated whether IL-4Rα expression on non-hematopoietic stromal cells (CD45$^-$) or hematopoietic cells (CD45$^+$) were important for mLN eosinophilia. To assess this, we constructed complete bone-marrow chimeras whereby IL-4Rα$^{-/-}$ recipient mice were given bone marrow from WT donor mice to generate mice lacking IL-4Rα on stromal cells (Fig-

ure S3C). In parallel, a cohort of WT mice (recipient) with IL-4Rα$^{-/-}$ mouse bone marrow (donor) were generated to analyze mice lacking IL-4Rα on CD45$^+$ hematopoietic cells (Figure S3D). After chimerism, mice were infected with *Hp*, and the whole mLN chain was harvested from mice at 21 dpi as well as from naive mice. In both bone-marrow chimera models, there was no eosinophilia (Siglec-F$^+$) in the paracortical region in naive mice (Figures S3C and S3D). At 21 dpi, eosinophilia was observed in the mice lacking IL-4Rα on stromal cells (Figure S3E) but not in mice lacking IL-4Rα on hematopoietic (CD45$^+$) cells (Figure S3F). Quantitative image analysis further confirmed that IL-4Rα expression on hematopoietic cells is required for the recruitment of eosinophils to the paracortical/IFR of the mLN (Figure S3G). Comparatively, in mice lacking IL-4Rα on stromal cells, we observed a significant increase in plasma cells in the paracortical T zone as well as at the cortical-medullary junction (Figures S4A–S4C, red insets). Additionally, in the paracortical region, the lack of eosinophils in mice lacking IL-4Rα on hematopoietic (CD45$^+$) cells (Figure S4B) correlated with the reduced number of plasma cells in this region (Figures S4B and S4C). Overall, these findings indicate that IL-4Rα expression on hematopoietic cells is important for the recruitment of eosinophils.

B cell-intrinsic IL-4Rα expression drives paracortical, cortical-medullary eosinophilia

Previous studies have shown that IL-4Rα expression on B cells is crucial for cortical region stromal remodeling,[19] yet the role of this pathway in mLN eosinophilia is unknown. Having confirmed that IL-4Rα expression on hematopoietic cells is important for the recruitment of eosinophils, we next investigated whether IL-4Rα expression on B cells was important for the recruitment of eosinophils into the mLN. To determine this, a mixed bone-marrow chimerism approach was used whereby WT mice were lethally irradiated and reconstituted with bone marrow from B cell-deficient mice (JhT$^{-/-}$) and IL-4Rα$^{-/-}$ mice to produce resultant mice that lacked IL-4Rα expression on B cells (JhT$^{-/-}$ + IL-4Rα$^{-/-}$, Figure S4D). As a control, WT mice received bone marrow from B cell-deficient mice (JhT$^{-/-}$) and WT mice (JhT$^{-/-}$ + WT, Figure S4E). We observed no apparent difference in the numbers of eosinophils in mice with IL-4Rα-deficient B cells and control mice under steady state (Figures S4D and S4E). No eosinophilia was observed in the paracortical region under steady state. At 21 dpi with *Hp*, mice lacking IL-4Rα expression on B cells failed to remodel the IFR as well as the paracortical region, which corresponded with reduced eosinophil numbers compared to mice that are sufficient for IL-4Rα on B cells (Figures 4A–4C). Quantitative flow cytometry experiments further confirmed the reduced accumulation of plasma cells

---

Figure 2. Non-hematopoietic stromal cells provide eosinophil chemoattractant to support mLN eosinophilia
(A–C) C57BL/6J (WT, green symbols) and IL-4Rα$^{-/-}$ (red symbols) mice were infected with *Hp*, and the entire chain of the mLN was collected at 0 (naive), 6 dpi, and 12 dpi. The total CD45$^-$ stromal fraction was isolated and used for gene-expression analysis. The relative expression of the major eosinophil chemoattractants, (A) *Ccl5*, (B) *Ccl11*, and (C) *Ccl24*, were analyzed using real-time PCR. Pooled data from two independent experiments with $n \geq 3$ mice per group are shown as mean ± SEM. *$p < 0.05$, **$p < 0.01$, ***$p < 0.001$, and ****$p < 0.0001$ (ANOVA, Bonferroni's multiple comparison test).
(D) Analysis of public gene expression database (Immgen.org) for eosinophil chemoattractant genes within the three most abundant stromal populations.
(E–G) mLN cryosections showing combined staining for DAPI (gray), ER-TR7$^+$ FRCs (blue), CCL24$^+$ (green), and Lyve1$^+$ LECs (red) in WT mice during (E) naive, (F) 12-dpi, and (G) 21-dpi *Hp* infection. In (F) and (G), white dotted insets show the enhanced CCL24 expression on Lyve1$^+$ vessels. Scale bars, 100 μm (E) and 20 μm (F, G).
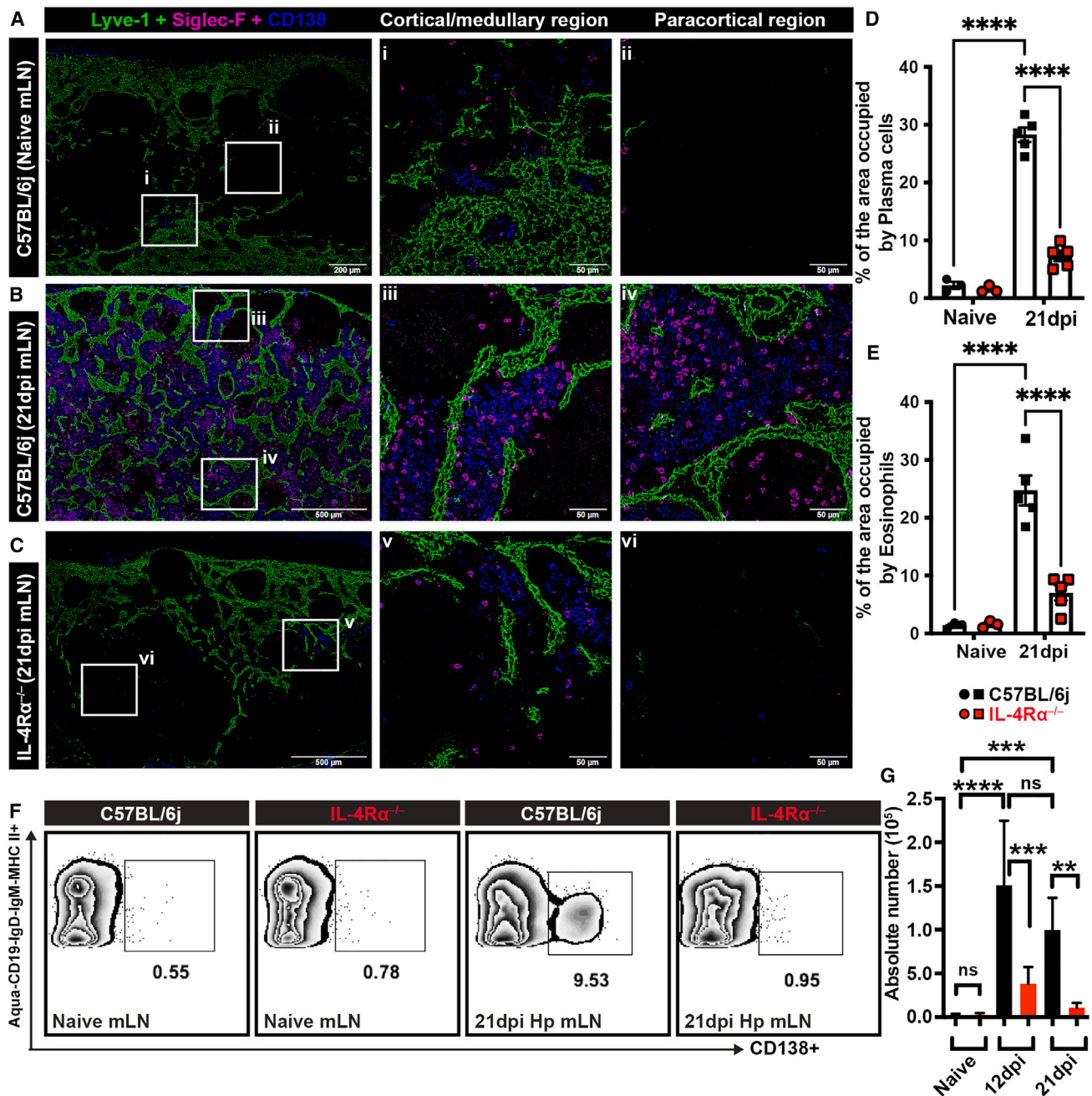
Figure 3. Cortical-medullary association of eosinophils with extrafollicular plasma cells requires IL-4Rα

C57BL/6J (black symbols) and IL-4Rα$^{-/-}$ (red symbols) mice were infected with *Hp*, and the entire chain of the mLN was collected at 0 (naive) and 21 dpi.

(A–C) (A and B) WT and (C) IL-4Rα$^{-/-}$ mLN cryosections showing combined staining for the CD138$^+$ plasma cells (blue), Siglec-F$^+$ eosinophils (magenta), and Lyve1$^+$ LECs (green). The white insets i, iii, and v highlight the cortical-medullary region, and insets ii, iv, and vi highlight the paracortical region. Images are representative of ≥ 3 different experiments with $n ≥ 2$–3 mice/group/time point. Scale bars. 200 μm (naive mLN) and 500 μm (*Hp* mLN). Scale bar in insets, 50 μm.

(D and E) Quantification of immunofluorescence images from the mLN of WT and IL-4Rα$^{-/-}$ mice showing percent area coverage by (D) CD138$^+$ cells and (E) Siglec-F$^+$ cells.

(F) Dot plots show the plasma cell population in the WT and IL-4Rα$^{-/-}$ naive and *Hp*-infected mLN.

(G) Absolute number of CD138$^+$ plasma cells in the mLN of naive, 12-dpi, and 21-dpi WT and IL-4Rα$^{-/-}$ mice.

Data represent mean ± SEM and are representative of two independent experiments with $n ≥ 2$–3 mice per infected group. ns, not significant; *$p < 0.05$, **$p < 0.01$, ***$p < 0.001$, ****$p < 0.0001$ (non-parametric Mann-Whitney U test).
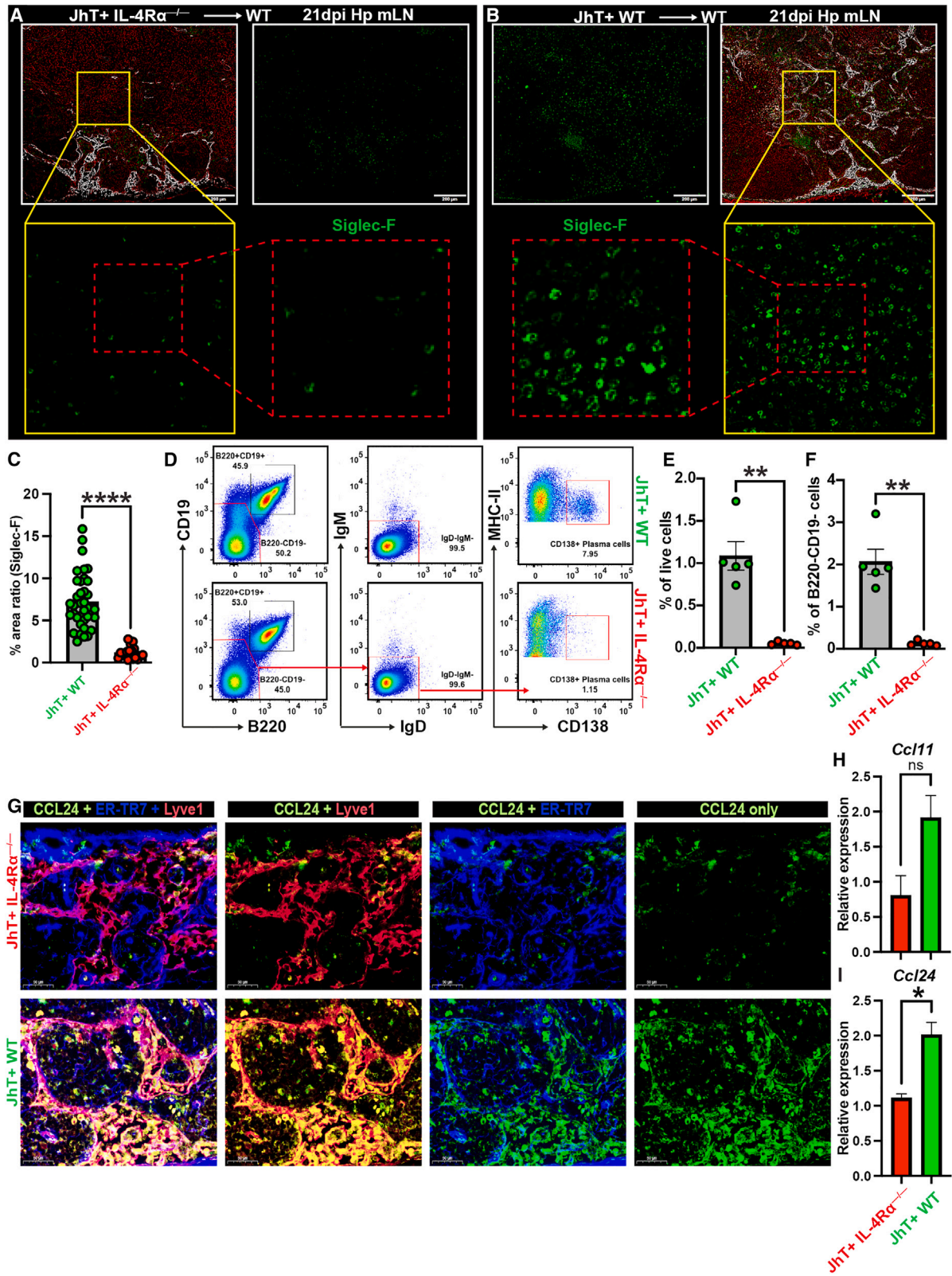
(legend on next page)

within the mLN (Figures 4D–4F), which correlated with reduced eosinophilia in mice that lacked IL-4Rα expression on B cells. Histological analysis of mLN strengthens our previous notion (Figure 3), highlighting the accumulation of CD138+ plasma cells at extrafollicular and cortical-medullary regions of the mLN (Figures S4F and S4G, red insets), which requires B cell-intrinsic IL-4Rα expression. Additionally, we observed significantly reduced expression of IL-5 (Figure S4H), CCL11, and CCL24 (Figures 4G–4I) within the mLN of mice lacking B cell-intrinsic IL-4Rα expression, which correlated with the lack of eosinophils and plasma cells in this region (Figure S4). Using these multidisciplinary approaches, our results confirmed that B cell-intrinsic IL-4Rα expression is important for the recruitment of eosinophils into the paracortical, interfollicular, and cortical-medullary regions of the mLN.

B cell-intrinsic lymphotoxin-β is required for mLN eosinophilia

Lymphotoxin-β (LTβ) is key to lymphoid organ development and architecture, and governs the infrastructure organization by supporting interactions between stromal cells and lymphocytes.[30] We have previously shown that IL-4Rα signaling on B cells drives LTα$_1$β$_2$ (lymphotoxin) upregulation, which then interacts with LTβR-expressing stromal cells to govern lymphoid stromal subset remodeling during helminth infection.[17] Having confirmed the role of IL-4Rα on B cells for driving eosinophilia into the mLN, we hypothesized that IL-4Rα-driven upregulation of lymphotoxin expression on B cells might be required for eosinophil recruitment to the mLN. To address the role of lymphotoxin-expressing B cells in driving mLN eosinophilia, we used a mixed bone-marrow chimera approach. WT mice were lethally irradiated and reconstituted with bone marrow from B cell-deficient (JhT$^{-/-}$, Figure 5A) or T cell-deficient (TCRβδ$^{-/-}$, Figure 5C) mice and mixed with bone marrow from LTβ$^{-/-}$ mice. The resultant mice lacked the expression of LTβ on either B cells (JhT$^{-/-}$ + LTβ$^{-/-}$, Figure 5A) or T cells (TCRβδ$^{-/-}$ + LTβ$^{-/-}$, Figure 5C). Control mixed bone-marrow chimeras were also generated using WT donors alongside LTβ$^{-/-}$ (JhT$^{-/-}$ + WT, Figure 5B) and TCRβδ$^{-/-}$ (TCRβδ$^{-/-}$ + WT, Figure 5D). The recipient mice were infected with Hp, and the mLN was collected at 21 dpi. Under steady-state conditions, we observed no apparent differ-ence in terms of lymphoid organization and numbers of eosinophils in LTβ-deficient B cells and LTβ-deficient T cells as well as in control mice (Figures S5A–S5D). Furthermore, no paracortical eosinophilia was observed in these animals. However, after Hp infection, mice that were selectively deficient for LTβ expression on B cells failed to expand the lymphatics network and were unable to recruit eosinophils into the interfollicular and paracortical regions of the mLN (Figure 5A). Higher-magnification images further confirmed reduced eosinophil association with cortical lymphatics (Figure 5E, white dotted insets). Comparatively, mice sufficient for LTβ on B cells (Figures 5B and 5F) were able to recruit eosinophils to the mLN and have an expanded lymphatics network following infection (Figure 5J). Mice that were LTβ deficient or sufficient on T cells had comparable eosinophilia (Figures 5C, 5D, and 5G–5I) and LEC expansion (Figure 5J) in the mLN following infection. Eosinophils were seen in close association with Lyve1+ LECs (Figures 5A and 5B), confirming that B cell crosstalk with stromal cells yields a favorable niche that supports eosinophil recruitment and interaction with stromal and immune cells within the mLN, further correlating with the accumulation of CD138+ plasma cells, which require LTβ expression selectively on B cells (Figures S5E–S5H). Furthermore, these results confirmed that LTβ expression on B cells and not T cells in response to Hp infection is crucial for the recruitment of eosinophils into the follicle-proximal regions of the mLN by supporting the expansion of the stromal network.

LTβR-activated FRCs enhance eosinophil activation and migratory capacity

Having established that eosinophils are present at the IFR and that the paracortical region was also in close proximity to B cells on the stromal scaffold, we hypothesized that eosinophil activation and gene expression were linked to their interaction with the activated stroma. To directly assess this hypothesis, we activated LTβR on cultured mLN FRCs using an agonist antibody (clone 4H8WH2) (Figure S6A, condition 1). Considering eosinophils have long been associated with providing B cell proliferative and survival factors,[26] we mimicked a cell-based activation model using purified naive B cells (Figure S6A, condition 2), given that B cell interaction with stroma can produce factors that can regulate eosinophil activation and migration. B cell-based

---

Figure 4. IL-4Rα-expressing B cells drive mLN paracortical/IFR eosinophilia through enhanced CCL24 expression by LECs

(A and B) Mixed bone-marrow chimeras were generated using lethally irradiated WT recipients reconstituted with (A) bone-marrow cells from B cell-deficient (JhT$^{-/-}$) mice mixed with bone-marrow cells from IL-4Rα$^{-/-}$ mice (JhT$^{-/-}$ + IL-4Rα$^{-/-}$), while (B) control mice received B cell-deficient bone marrow mixed with WT cells (JhT$^{-/-}$ + WT). All mice were infected with Hp, and the mLN was collected at day 0 (naive) and 21 dpi for analysis. mLN cryosections from JhT$^{-/-}$ + IL-4Rα$^{-/-}$ and control mixed bone-marrow chimeric infected mice underwent immunofluorescence image staining for Lyve1+ (white), Pdpn+ (red), and Siglec-F+ (green). The magnified view of the paracortical region (yellow and red insets) from 21-dpi mLN highlighting eosinophilia is shown for both groups in a side-by-side comparison. The red insets show a higher magnification of Siglec-F+ cells (green) within the paracortical region. The images are from representative mice and from two independent experiments with n ≥ 2–4 mice per group. Scale bars, 200 μm.

(C) Quantification of immunofluorescence images from the mLN showing percent area ratio by Siglec-F+ cells. Total length of the mLN was segmented for cortical vs. paracortical region and analyzed for Siglec-F+ cells across the length of mLN. n = 18 JhT$^{-/-}$ + IL4Rα$^{-/-}$ and n = 37 images for control group. Data represent mean ± SEM and are representative of n ≥ 3 mice per infected group.

(D–F) (D) Pseudocolor dot plots and (E and F) histograms showing the percentage of live cells and percentage of CD138+ plasma cell population in JhT$^{-/-}$ + IL-4Rα$^{-/-}$ and control mice mLN at 21 dpi.

(G–I) (G) mLN cryosections showing combined staining for ER-TR7+ FRCs (blue), CCL24+ (green), and Lyve1+ LECs (red) in chimeric mice at 21-dpi Hp infection. Scale bars, 100 μm and 20 μm. Total RNA was isolated from whole mLN of JhT$^{-/-}$ + IL-4Rα$^{-/-}$ and control mice, and (H) Ccl11 and (I) Ccl24 gene expression was analyzed using RT-PCR. Data represent mean ± SEM and are representative of two independent experiments with n ≥ 2–3 mice per infected group.

ns, not significant; *p < 0.05, **p < 0.01, ***p < 0.001, ****p < 0.0001 (non-parametric Mann-Whitney U test).
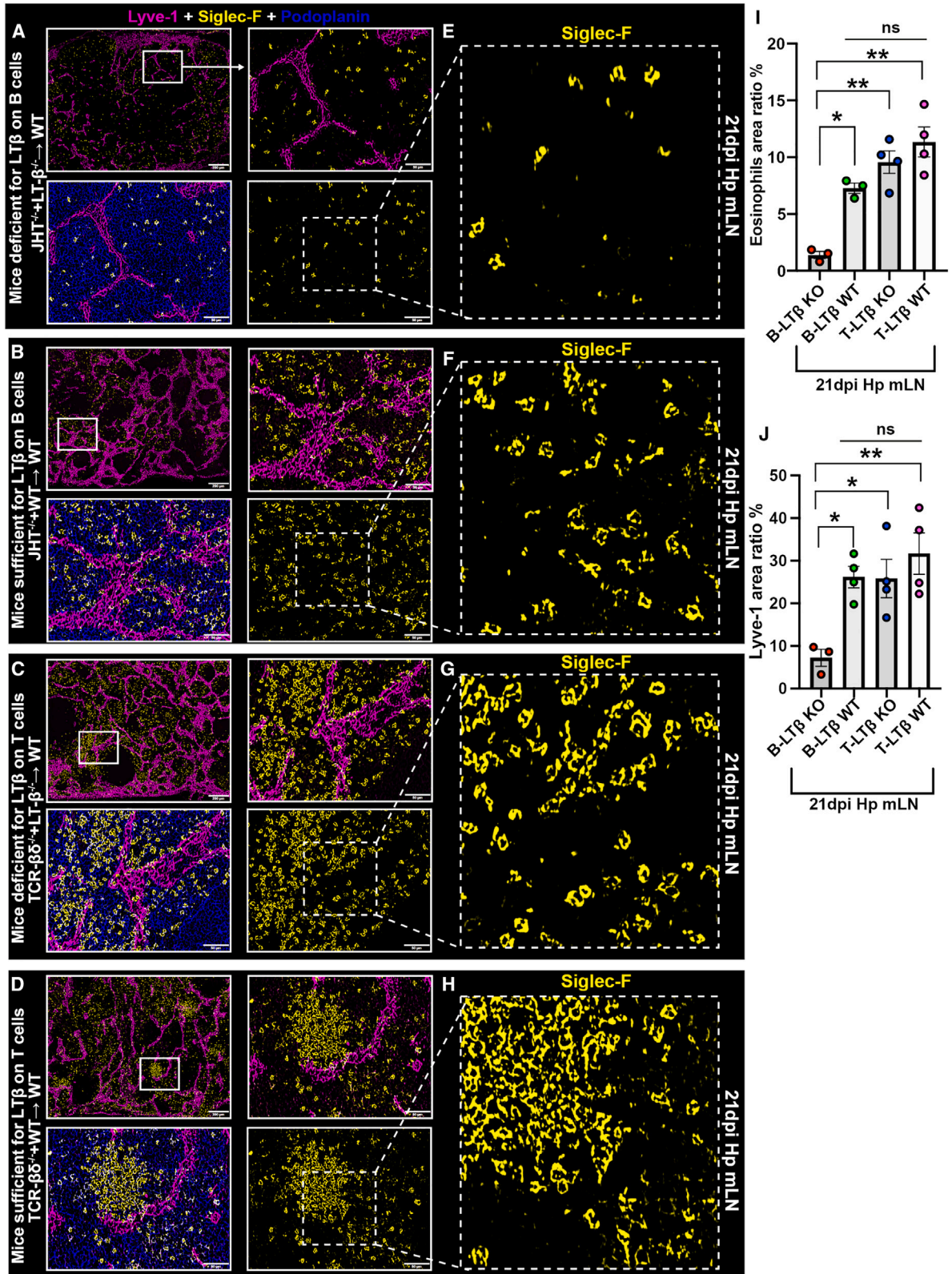
(legend on next page)

activation as well as agonist antibody-based activation resulted in an activated FRC phenotype and were later used for co-culture with bone-marrow-derived eosinophils. After 8 h of co-culture with activated FRCs the eosinophils were purified, and bulk RNA sequencing was performed to identify global changes in their transcriptomes. We identified that eosinophils co-cultured with B cell-activated FRCs had a greater enrichment of *MhcII*, *Ccr7*, *Il6*, and *Il1β* (Figures S6B–S6E) in comparison to cells co-cultured with non-activated FRCs. These observations suggested that the interaction of B cells with FRCs provides additive factors that enhance eosinophil activation as well as their ability to prime B cells. Since extracellular activation of eosinophils is regulated through the nuclear factor κB (NF-κB) signaling pathways,[16] we performed subsequent analysis to assess the expression of NF-κB signaling components—*Nfkbie*, *Relb*, *Nfkb1*, *Nfkbib*, *Rela*, *Nfkb2*, and *Nfkbiz*—in eosinophils obtained from the co-culture. In both conditions, comparable NF-κB activation was observed (Figures 6A and 6B). We further analyzed various known functional modules such as tissue repair, degranulation, and adhesion molecules (Figures 6C–6E), as well as cytokines, chemokines, and immunoglobulin receptors (Figures S6F–S6H), which are all important for eosinophil function. Gene expression between the two groups remained mostly conserved. Analysis of cytokine/chemokine receptors showed an enrichment of the ST2 (*Il1rl1*) receptor along with *Il5ra* and *Tnfrsf1a* (target gene for STAT3) in eosinophils that had been co-cultured with LTβR-activated FRCs (Figure 6F).

We next performed STRING analysis to find putative direct and indirect interactions on these genes. The STRING analysis yielded a total of 31 biological processes based on gene ontology (GO) (Table S1). We focused on proteins relating to the regulation of IL-5 production (GO:0032674), considering IL-5 is one of the key survival factors for eosinophils. Out of 22 known proteins within the network (Figure S6I), STRING analysis predicted association and/or co-occurrence between the ST2 receptor (*Il1rl1*) and *Il5ra* within our network that could be linked to receiving survival signals from both IL-5 and IL-33 (Figure 6G). The wider network representation further highlights a distinct cluster of proteins where eosinophil peroxidase (EPX) was also associated with IL5Rα and IL-33 (Figure S6I), suggesting that IL-33 may also be involved with eosinophil immune functions and survival.[31,32] The association of eosinophils with the stromal cells within the mLN and co-occurrence of the ST2 receptor (*Il1rl1*) and *Il5ra* within our network analysis led us to hypothesize that FRCs may support the eosinophil function by producing a ligand for *Il1rl1*, i.e., IL-33, and whether B cells may induce IL-

33 expression in FRCs. First, we validated these hypotheses in relation to IL-33 expression using our co-culture system where FRCs were activated through LTβR signaling. Ligation of LTβR using an agonist antibody enhanced the *Il33* expression in FRCs, which was further enhanced by lymphotoxin-expressing B cells (Figure 6H). The activated phenotype of FRCs was confirmed by analyzing *Icam1* gene expression (Figure 6I), in line with previous reports.[33]
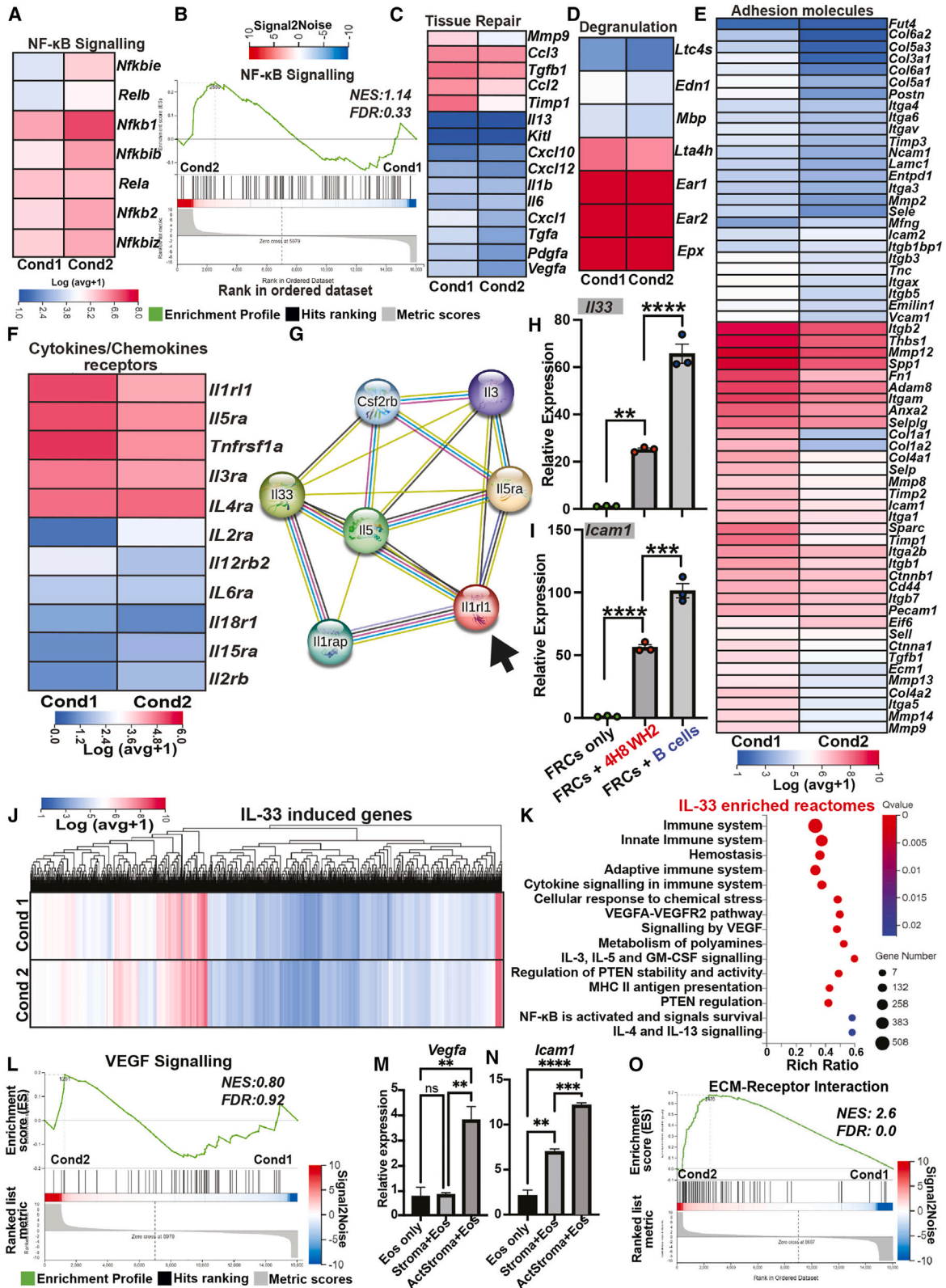
Second, we evaluated whether stromal-derived IL-33 may alter the transcriptomic profile of eosinophils. To explore whether activated FRCs may modulate the eosinophil transcriptional signatures reported to be induced by IL-33, we performed a targeted analysis of our sequencing data based on published datasets[16,34] of known IL-33-induced genes in eosinophils (GEO: GSE43660 and GSE182001) and identified 4,757 genes (with fragments per kilobase per million [FPKM] value >1) that were enriched in our dataset (Figure 6J). We found no distinguishable difference in the gene-expression pattern between the two stromal cell activating conditions. Highly enriched IL-33-induced genes (with an FPKM ≥5; 3,649 transcripts) were analyzed using the Reactome database to gain insight into the key pathways that were being upregulated in eosinophils (Figure 6K). Reactome pathways that were significantly enriched in an IL-33-specific manner in eosinophils stimulated by activated FRCs included the vascular endothelial growth factor A (VEGF-A), VEGFR2 pathway, and VEGF signaling (Figures 6K and 6L). These pathways have been reported to enhance eosinophil activation by modulating their chemotactic and degranulation activity.[35] Validation by RT-PCR confirmed that *Vegfa* expression was significantly increased in eosinophils that had been co-cultured with LTβR-activated FRCs (Figure 6M). Both gene-expression analysis and bulk RNA sequencing also showed that eosinophils co-cultured with activated stroma had increased expression of *Icam1* (Figure 6N) and a higher expression of adhesion molecules involved in extracellular matrix-receptor interactions (Figure 6O) and focal adhesion (Figure S6J). This suggested that stromal-cell-derived IL-33 can promote eosinophil accumulation within the mLN through enhancing chemotaxis as well as cell-matrix adhesion. Additionally, other enriched reactomes included hemostasis, IL-3, IL-5, and GM-CSF (granulocyte macrophage colony-stimulating factor) signaling, and IL-4 and IL-13 signaling (Figure 6K), which are linked to tissue repair (Figure 6C), degranulation (Figure 6D), and platelet activation (Figure S6K) as well as promoting the adaptive immune response through antigen processing and presentation (Figure S6L), suggesting that stroma not only provide a

Figure 5. Lymphotoxin-expressing B cells govern mLN eosinophilia

(A–D) Mixed bone-marrow chimeras were generated as described in STAR Methods. Chimeric mice lacking lymphotoxin expression distinctly on either (A) B cells (JhT$^{-/-}$ + LTβ$^{-/-}$) or (C) T cells (TCRβδ$^{-/-}$ + LTβ$^{-/-}$) were compared to respective control mice having (B) B cells or (D) T cells sufficient for lymphotoxin, JhT$^{-/-}$ + WT and TCRβδ$^{-/-}$ + WT, respectively. All chimeric mice were infected with *Hp*, and the mLN was collected at 21 dpi.

(E–H) Infected chimeric mice lacking lymphotoxin on (E) B cells (JhT$^{-/-}$ + LTβ$^{-/-}$) and their respective controls (JhT$^{-/-}$ + WT) (F) with immunofluorescence staining for Pdpn$^+$ (blue), Siglec-F$^+$ (yellow), and Lyve1$^+$ (magenta). Infected chimeric mice lacking (G) lymphotoxin on T cells (TCRβδ$^{-/-}$ + LTβ$^{-/-}$) and respective controls (TCRβδ$^{-/-}$ + WT) (H) showing eosinophilia (yellow cells) along the LEC network (magenta). The white inset shows a higher-magnification view of Siglec-F$^+$ cells (yellow) in close vicinity to the interfollicular region. Scale bars, 200 μm and 50 μm.

(I and J) Quantification of immunofluorescence images from the mLN showing percent area ratio by (I) Siglec-F$^+$ cells and (J) Lyve-1$^+$ cells. Eosinophil accumulation within the mLN across the four groups highlight the significantly reduced percent area for Siglec-F$^+$ cells in mice lacking lymphotoxin expression on B cells. Data represent mean ± SEM with $n \geq 3$–4 mice per group. ns, not significant; *$p < 0.05$, **$p < 0.01$, ***$p < 0.001$, ****$p < 0.0001$ (ANOVA, Bonferroni's multiple comparison test).

A NF-κB Signalling

B NF-κB Signalling — NES:1.14 FDR:0.33

C Tissue Repair

D Degranulation

E Adhesion molecules

F Cytokines/Chemokines receptors

G

H Il33

I Icam1

J IL-33 induced genes

K IL-33 enriched reactomes

L VEGF Signalling — NES:0.80 FDR:0.92

M Vegfa

N Icam1

O ECM-Receptor Interaction — NES: 2.6 FDR: 0.0

(legend on next page)

suitable niche for eosinophil recruitment but can possibly support their survival as well as modulate their immune function within the mLN microenvironment. Based on these findings, we hypothesized that IL-4-IL4Rα-driven lymphotoxin upregulation on B cells can ligate LTβR on FRCs, which in turns can lead to IL-33 expression within the mLN.

To provide experimental evidence for this line of events within the mLN, we performed *in vivo* validation using mixed bone-marrow chimeras from mice that are sufficient or deficient for IL-4Rα on B cells (refer to Figure 4). The total mLN analysis showed significantly reduced *Il33* expression in the mLN of helminth-infected mice lacking IL-4Rα on B cells (Figure S6M). Immunofluorescence microscopy using mLN cryosections indicated reduced IL-33 expression in 21-dpi mice lacking IL-4Rα on B cells (Figures S6N–S6O), which was linked with a lower frequency of eosinophils in the follicle-proximal regions of the mLN. Overall, these results establish a key role of B cell-stromal crosstalk in driving IL-33 expression and the recruitment of eosinophils into the follicle-proximal regions of the mLN during helminth infection. Furthermore, these results highlight a previously unidentified role of activated FRCs and the niches they create by interacting with B cells within the mLN, which can possibly promote eosinophil survival, activation, and alteration in gene expression.

LTβR engagement on CCL19^cre+ FRCs enhances IL-33 expression, tissue eosinophilia, and their survival

We next aimed to confirm the importance of LTβR engagement on FRCs in supporting eosinophilia into the mLN as well as validate the role of LTβR in driving IL-33 expression *in vivo*. To assess this, we used mice that have Cre-recombinase expression under the control of the *Ccl19* promoter,[36] which were crossed to LTβR^fl/fl mice resulting in a selective deletion of LTβR on CCL19^+ stromal cells. *Hp* infection of Cre^+ (CCL19^Cre+ × LTβR^fl/fl or LTβR^−/−) mice showed a decreased number of eosinophils within the mLN compared to Cre^− (CCL19^Cre− × LTβR^fl/fl or LTβR^+/+) controls (Figures 7A and 7B). Histological analysis further endorsed our previous findings (Figure 6), highlighting that LTβR signaling in FRCs governed the IL-33 expression by stromal cells (Figures 7C and 7D). Interestingly, we observed a significantly enriched accumulation of IL-33 on the ER-TR7^+ reticular network in LTBR^+/+ mice (Figure 7C, blue insets, red arrows), suggesting an enhanced release from the FRCs, especially at the eosinophil-enriched IFR (Figure S7A). Additionally,

the mLN of LTβR^−/− mice showed reduced IL-33^+ FRCs, but not Lyve1^+ LECs (Figures 7C–7E and S7D) at the cortical IFR, which also correlated with the lack of eosinophils (Figure 7A) and plasma cells in this region (Figures S7B and S7C). This further highlighted the division of labor between the two distinct stromal subsets, i.e., FRCs and LECs in tissue eosinophilia, with the former providing the survival factors (IL-33) while later providing the chemoattractant (CCL24).

Additionally, the direct role of FRCs in supporting eosinophil survival was confirmed *in vitro*. We cultured bone-marrow-derived eosinophils in the presence or absence of activated FRCs and measured cell viability by staining CD11b^+Siglec-F^+ eosinophils with DAPI, followed by flow cytometry. Notably, the presence of FRCs within the co-culture significantly enhanced eosinophil survival over time (Figure 7F) and their activation as evaluated by CD11b expression (Figure 7G). Although LEC-derived chemoattractant confirmed their contribution in cellular trafficking, we could not establish the direct contribution of LECs in eosinophil survival due to low yield of purified LECs from the mLN. Nevertheless, global analysis of the entire mLN chain further confirmed the reduced number of total IL-33^+ nuclei in LTβR^−/− (n = 19,254) compared to LTβR^+/+ (n = 52,859) mice (Figure S7A, second panel from left for IL-33 only). Overall, these results highlight the directive role of FRCs in eosinophil recruitment, survival, and activation within the mLN niches in the context of type 2 immunity.

Eosinophil synergizes with stromal subsets to drive IL-33 expression and host response

Having established the direct role of lymphoid stroma (specifically FRCs and LECs) in eosinophil recruitment, survival, and activation, we next studied the reciprocal effect of eosinophil on stromal gene expression as well as their contribution to the anti-helminth response. We infected WT and eosinophil-deficient ΔdblGATA-1 mice[37] to validate these interactions *in vivo*. Helminth infection induced an increase in the total weight (a surrogate for cellularity) of the mLN in 21-dpi WT but not in 21-dpi ΔdblGATA-1 mice (Figure 7H), a change that was, however, not observed at an earlier time point after infection (12 dpi) and in other secondary lymphoid organs, i.e., spleen (Figures S7E and S7F). Evaluation of worm burdens at 12 dpi in ΔdblGATA-1 mice compared with WT controls showed no significant difference, suggesting that the development of L3 larvae to adult worms as well as their emergence to the intestinal lumen is not

---

Figure 6. LTβR-activated FRCs enhance eosinophil activation and immunomodules

LN-derived stromal cells and bone-marrow-derived eosinophils were generated *in vitro* as described in STAR Methods. Eosinophils were co-cultured with activated stromal cells and later analyzed using bulk RNA sequencing.

(A and B) (A) Heatmap and (B) gene set enrichment analysis (GSEA) plot showing expression of genes linked to NF-κB signaling.

(C–F) Heatmaps showing genes relating to (C) tissue repair, (D) degranulation, (E) adhesion molecules, and (F) cytokine/chemokine receptors.

(G) STRING analysis was performed on cytokine receptors. STRING network shows cytokine receptors within the regulation of "IL-5 production" gene ontology pathway (GO:0032674). Known interactions are indicated by cyan (curated database) and magenta (experimentally determined), and predicted interactions are indicated by black (co-expression), green (text mining), dark blue (gene co-occurrence), and lilac (protein homology). Data are from representative independent experiment and presented as mean ± SEM.

(H and I) Activation of FRCs by LTβR ligation or via co-culture with B cells showing the relative expression of (H) *Il33* and (I) *Icam1* expression.

(J) Heatmap showing IL-33 analysis based on GEO: GSE43660 and GEO: GSE182001 datasets with FPKM ≥ 1.

(K) Reactome bubble chart representing 15 Reactome pathways of highly enriched IL-33 induced genes (FPKM ≥ 5).

(L–N) (L) GSEA plot and (M) *Vegfa* and (N) *Icam1* expression in eosinophils co-cultured with LTβR stromal cells.

(O) GSEA plot showing ECM receptor interaction highlighting eosinophil association with FRCs.

ns, not significant; *p < 0.05, **p < 0.01, ***p < 0.001, ****p < 0.0001 (one-way ANOVA, Bonferroni's multiple comparison test).
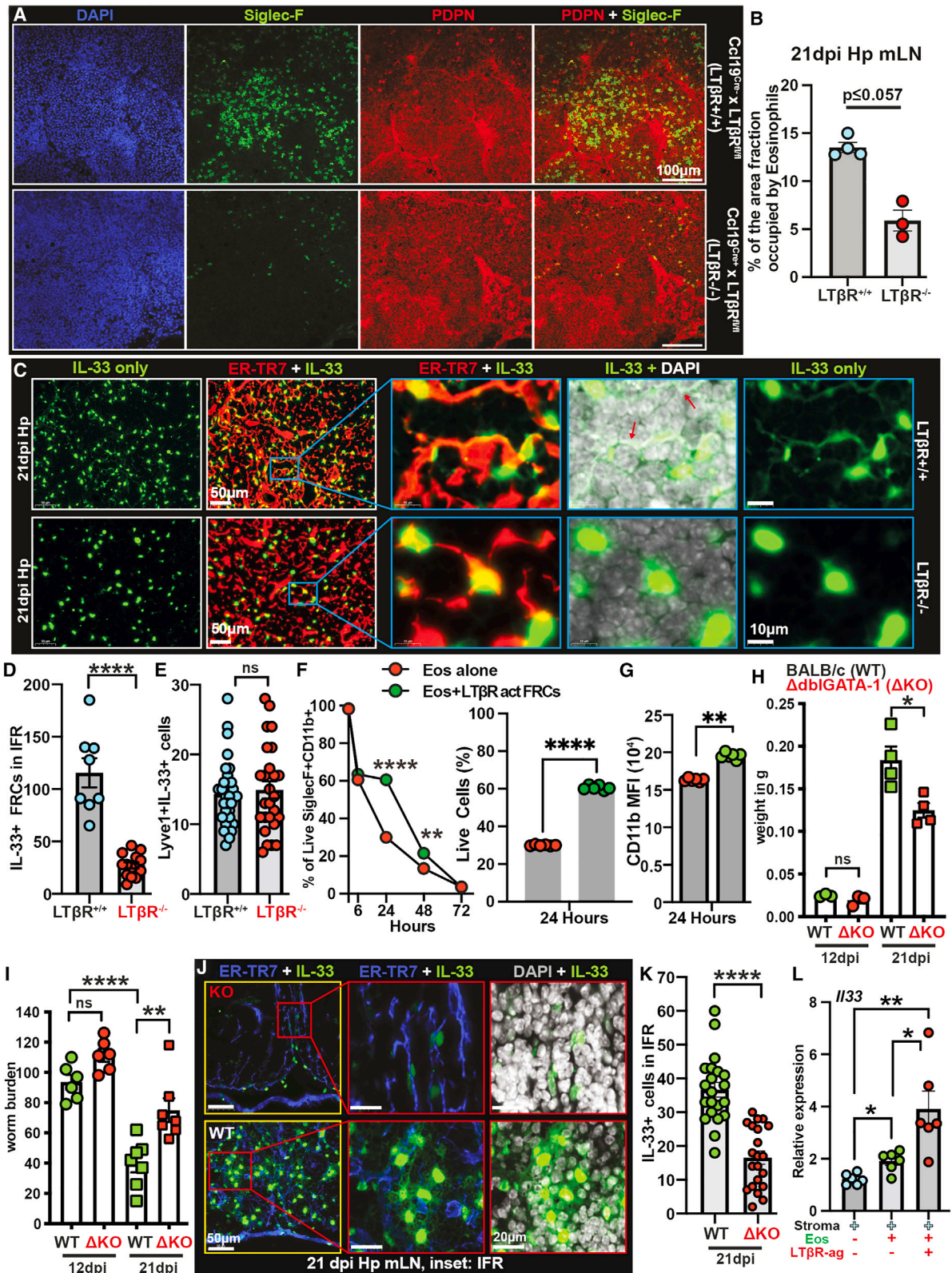
(legend on next page)

impacted by the absence of eosinophils. However, at the later stage of infection we found a significant difference in the worm burden between WT and ΔdblGATA-1 mice (Figure 7I). Analysis of IL-33 expression in mLN of 21-dpi WT and ΔdblGATA-1 mice showed significantly reduced IL-33 expression at the IFR compared to WT counterparts (Figures 7J and 7K).

To corroborate these results, we performed *in vitro* co-culture experiments to determine whether eosinophils play a synergistic role in stromal activation and IL-33 expression. The enriched CD45− stromal fraction contained a mixture of FRCs and LECs, as described previously,[38] thus allowing us to study the *Il33* and *Ccl24* expression in these subsets simultaneously. In agreement with our *in vivo* findings in ΔdblGATA-1 mice, we observed that eosinophils significantly induced *Il33* and *Ccl24* but not *Il6* expression in LN-derived stroma (Figures 7L and S7G), which was further enhanced when stromal cells were pre-activated with LTβR agonist antibody mimicking B cell-stromal crosstalk. Taken together, these results indicated that eosinophils can additionally regulate the lymphoid stromal subset gene expression in a synergistic manner that can be linked to stroma-derived IL-33 and CCL24, which are known to be a strong driver of Th2 immunity.[39,40]

In summary, by using *Hp* as a model organism, we provide a mechanistic view of eosinophil recruitment to the secondary lymphoid organ and highlight a novel role of B cell-stromal cell dialogue in this process. IL-4-driven lymphotoxin upregulation enhanced B cell crosstalk, with LTβR+ stromal cells leading to enhanced eosinophil recruitment, activation, and survival. Eosinophils in turn can interact with B cells and lymphoid stroma to drive additional cytokine/chemokine secretion in a positive feedback manner to support the development of a humoral response (Figure S7H). Furthermore, our results highlight the complexity within the lymphoid compartment and open new doors to the study of potential interactions between eosinophils and stromal cells in diverse immunological settings.[23,41,42]

DISCUSSION

The role of stromal cells in eosinophil recruitment to the mLN expands the central paradigm of lymphoid non-hematopoietic stroma, which was previously largely associated with the survival, migration, and function of B cells, T cells, and DCs.[3,4,43] Utilizing *Hp* as a model organism, we have elucidated the intricate mechanism behind the recruitment, sustenance, activation, and functionality of eosinophils within the secondary lymphoid tissues draining the gastrointestinal tract.

Our results suggest that helminth-induced mLN stroma activation and remodeling via IL-4-IL4Rα-driven B cell lymphotoxin upregulation[17,44] can provide the necessary infrastructure and cytokine/chemokine expression for the recruitment, survival, and retention of eosinophils, which is in line with previous work.[12,45,46] The presence of eosinophils in close association with extrafollicular CD138+ plasma cells strengthens their supporting role toward the humoral response,[26] which is the key to drive protection against helminths.[28,47] Hematopoietic cells expressing IL-4Rα are key to mounting a protective immune response against nematodes[20,47] where IL-4Rα-expressing B cells drive the expansion and remodeling of stromal subsets, which regulates B cell localization and follicle formation.[19] This further emphasizes the importance of stromal-immune cell interaction toward an enhanced type 2 response by recruiting and repositioning immune cells at immune interactive sites within the lymphoid organ.[17,29,48]

Immune cell positioning by LN stromal cells is key to a rapid T cell response[48] as well as B cell survival, follicle formation, and function.[3,17] Therefore, exploring the cellular constituents at the IFR and T/B border, which are important immune niches, will be crucial to determining the spatial cellular diversity in these sites. The IFR lies between the B cell follicles and the T cell zone and is where B cells, T cells, and DCs interact to generate the adaptive immune response.[29] We have previously demonstrated that B cells are present within the close vicinity of LECs lining the IFR in the Th2 microenvironment,[24] and others have shown that B cells are capable of producing IL-4 requiring IL-4Rα.[49] Our results strongly suggest that eosinophil recruitment and association with CCL24-producing LECs and B cells can be, at least in part, a result of B cell-derived IL-4 directly acting upon LECs and FRCs, thus driving CCL11 and CCL24 expression.[50] Therefore, we propose that IL-4-producing B cells, generated in response to infection,[49] may serve to amplify eosinophilia by

Figure 7. Loss of LTβR on CCL19cre+ FRCs attenuates IL-33 expression and eosinophilia

CCL19cre+ or Cre− × LTβRfl/fl mice were infected with *Hp*, and mLNs were collected at 21 dpi.

(A and B) mLN cryosections from mice at 21 dpi showing combined immunofluorescence staining for Siglec-F+ eosinophils (green) and Pdpn+ stroma (red) along with DAPI are shown. (B) Percentage of area occupied by Siglec-F+ cells in LTβR+/+ (CCL19Cre− × LTβRfl/fl) and LTβR−/− (CCL19cre+ × LTβRfl/fl) mice enumerated across the entire chain of mLN. Data are representative of at least two independent experiments and are presented as mean ± SEM. Histogram with dot plot is presented as mean ± SEM with n ≥ 3–4 mice per group.

(C) Immunofluorescence staining of LTβR+/+ and LTβR−/− mLN at 21-dpi *Hp* infection highlighting the nuclear vs. non-nuclear IL-33 (green) expression by FRCs (ER-TR7+; red). Released IL-33 on stromal reticulum is highlighted by red arrow.

(D and E) Quantification of total IL-33+ FRCs and IL-33+LECs at the IFR.

(F and G) Eosinophil survival assay showing percentage of live eosinophils cultured alone (red dots) or in presence of LTβR-activated FRCs. Eosinophils showed (F) higher survival rate and (G) higher CD11b expression reflecting heightened activation in the presence of activated FRCs post 24 h of culture. Eosinophils can drive IL-33 expression by lymphoid stroma, which is enhanced in the presence of activating signals.

(H–K) Loss of eosinophils leads to reduced IL-33 expression by stromal cells and a higher worm burden. (H) *Hp*-infected WT and ΔdblGATA-1 mice mLN weight at 21 dpi. (I) Adult worm burden in WT (green) and ΔdblGATA-1 mice (red) at day 12 and day 21 post primary *Hp* infection. Each dot represents an individual mouse. (J) Immunofluorescence staining showing IL-33+ FRCs at the IFR in BALB/c (WT; green bars) and ΔdblGATA-1 (ΔKO; red bars) mice mLN. (K) Quantification of IL-33+ FRCs at the IFR as described above (C and D). Data represent mean ± SEM from two independent experiments (pooled) with n ≥ 3–4 mice per group/time point. ns, not significant; *p < 0.05, **p < 0.01, ***p < 0.001, ****p < 0.0001 (ANOVA, Bonferroni's multiple comparison test).

(L) Relative expression of *Il33* in CD45-stroma after 24 h of co-culture with eosinophils. Two independent experiments (in triplicate) were pooled, and data represent mean ± SEM. *p < 0.05, **p < 0.01, ***p < 0.001, ****p < 0.0001 (non-parametric Mann-Whitney U test).

activating and polarizing LECs via B cell-intrinsic IL-4Rα signaling, which can directly support the secretion of eosinophil chemoattractant. Immgen analysis indicated the differential expression of CCL11 and CCL24 within the stromal subsets. These chemoattractants have been previously shown to be an important player in type 2 immunity[40,51]; therefore, the reduced CCL24 expression in IL-4Rα^{−/−} mice can be indirectly linked to the reduced availability of chemoattractant resulting from defective LEC expansion[24] and activation. In contrast, studies have shown that Th2 cytokines and IL-4Rα signaling have an anti-lymphangiogenic effect[52] whereas helminth infection drives an enhanced mLN LEC expansion.[24] Therefore, a more detailed analysis of LEC expansion in IL-4Rα^{−/−} mouse mLN is required to establish the differential regulation between peripheral LNs vs. mesenteric LNs[44] as well as establishing a direct link from IL-4Rα, B cells, and eosinophilia to lymphangiogenesis during acute and/or chronic inflammation. Nevertheless, the reduced LEC numbers seen in infected LTβR^{−/−} mice[24] can be directly linked to the reduced CCL24 and associated eosinophilia. These results further strengthen the functional role of eosinophils in diverse immunological settings from cancer to thymus regeneration, where IL-4Rα plays a key supporting role by modulating stromal cell function.[23,42,50,53]

Interestingly, the loss of LTβR on FRCs resulted in reduced IL-33 expression as well as their presence on non-nuclear reticular fibers. This can be associated with the active release of IL-33,[54,55] yet the mechanism behind such processes in FRCs remains unknown and requires further investigation. Our results suggested that the enhanced expression of IL-33 within the lymphoid niches can amplify type 2 signaling along with synthesis and release of IL-5 from innate lymphoid cells (ILCs) including lymphoid tissue-inducer cells (LTi cells), which often accumulate at the IFR after *Hp* infection in a CCR7-dependent manner.[56] This cooperative interaction could sustain the mLN eosinophilia for a longer duration.[22] The presence of CCR7 on eosinophils highlights their migratory potential from the periphery to the lymphoid compartment, as seen previously in allergic inflammation.[57,58] This suggests that stroma-derived eosinophil chemoattractants (CCL11 and CCL24) and survival factor (IL-33) along with CCR7 ligands, CCL19 and CCL21, can operate in synergy to localize these granulocytes to distinct regions of the mLN where DC clustering, antigen presentation, and T cell and B cell activation take place. It is important to note that the IFR and corticomedullary region are sites that allow entry and exit for naive lymphocytes[1]; therefore, the presence of both eosinophils and plasma cells within these sites can enhance the T cell activation. However, the route and mechanisms of this migration and antigen presentation are not yet well defined and would require further investigation.

Our findings further strengthen the hypothesis that stromal cells not only regulate local B cell survival but may also indirectly regulate the peripheral population by recruiting eosinophils from the tissue to the mLN, which allows these effector cells to migrate back into circulation followed by homing to the desired niches. The lymphotoxin-activated FRC-eosinophil co-culture highlights the capability of activated FRCs to modulate both MHC-II (major histocompatibility complex II) expression as well as ICAM-1 (intercellular adhesion molecule 1) expression in eo-

sinophils. A possible mechanism of such regulation could be that FRC-derived IL-33 directly programs eosinophil ICAM-1 expression.[59] The upregulation of ICAM-1 on eosinophils and their presence at the IL-33-enriched IFR of the mLN further strengthens the notion that eosinophils might provide an additional scaffold at these sites for B cell adhesion and synapse formation, as previously reported.[60] The association of eosinophils with vasculature and FRCs further hints that ICAM-1 supports VEGF-A-mediated chemotaxis,[61] and previous reports have shown that IL-33-induced ICAM-1 expression enhances adhesiveness of eosinophils.[31,62,63]

Considering the high levels of IL-4, IL-5, and IL-33 and the constant presence of eosinophils within the mLN over the time course of infection suggests that the lymphoid microenvironment provides a suitable survival niche for granulocytes.[8,20] This also explains the synergistic role of eosinophils by positively regulating cytokine/chemokine expression by stromal cells, possibly via the lymphotoxin pathway, which is downregulated in ΔdblGATA-1 mice.[64] This further suggests that redundant signals can modulate FRC niches within the lymphoid tissues after inflammatory response in a positive feedback or feedforward manner to support the ongoing immune response. Interestingly, CCL11, which is highly enriched in FRCs but not in LECs, drives eosinophil granule mobilization and secretion, resulting in the release of IL-4 and IL-4Rα,[65] and is also reported to be associated with adipose eosinophilia.[50] This indirectly highlights the potential of FRCs in regulating granulocyte degranulation processes and associated release of Th2 cytokines at the IFR, thereby sustaining a type 2 immune microenvironment. The capability of eosinophils to produce IL-4 against parasitic antigens[66] and potential to induce IL-33 and CCL24 by stromal subsets collectively demonstrates their significance to enhance the ongoing Th2 response within the IFR for a longer duration, supporting previous findings in which stroma-derived signals play a key role.[29,50]

While eosinophilia appears to be dispensable for the anti-helminth response in a helminth context,[12,22,47,67] our results using *Hp* as a model helminth suggest that the eosinophils contribute toward stromal activation and development of the Th2 response within the mLN, likely through CCL24 and IL-33-driven Th2 cytokine expression,[39] leading to host protection toward the later stages of infection. It is important to note that our study does not eliminate the contribution of other immune cells that are also present within the IFR or T/B border[29] and were previously demonstrated to be important for the anti-helminth response, which requires eosinophils and CCL24.[40,47] Furthermore, eosinophils could simply pass through the mLN to enter circulation and subsequently migrate to mucosal tissues such as the lung, small intestine, and adipose tissue, where they regulate tissue homeostasis[50,68] as well as performing effector functions in infection/inflammatory settings.[10]

Our findings also indicate that eosinophils have the capacity to influence FRC gene expression. However, the role of eosinophils/granulocytes in directly regulating the function of distinct stromal subsets—FDCs, T-zone reticular cells (TRCs), marginal reticular cells (MRCs), and B cell zone reticular cells (BRCs)—that primarily construct the distinct lymphoid niches[5] is not fully understood and requires detailed investigation. An unprecedented analysis by Cui et al. highlights the cytokine-mediated

cell-cell interactome for FRCs,[69] showing their capability to influence almost every immune population despite eosinophils being under-represented. Therefore, our study provides the bridging link to the role of FRC-derived cytokines that has the capability to modulate cellular function of nearly all cell types, including eosinophils within the lymphoid as well as in the non-lymphoid microenvironment.[69]

In conclusion, our results identify an intricate relationship between B cells and stromal cells in the recruitment of eosinophils to various immune interactive niches within the mLN. Our study further extends the current paradigm about LN stromal cells and highlights that lymphoid stroma can govern the recruitment, survival, migration, and function of not only lymphocytes and myeloid cells but also eosinophils, which are instrumental to gastrointestinal tract and host defense.[9]

Limitations of the study

Although our study provides compelling evidence of B cell-stromal crosstalk for eosinophil recruitment and survival driven by CCL24 and IL-33 from lymphoid stromal subsets, the direct contribution of FRC-derived IL-33 remains to be determined. The current study lacks the *in vivo* ablation of stromal-cell-intrinsic IL-33 or eosinophil chemoattractants in FRCs and LECs, which would require the development of novel genetic tools to dissect the relative contributions of each stromal subset and warrants future investigation. Furthermore, the parasite penetrates the intestinal wall causing significant tissue damage, which could result in the expression as well as release of IL-33. Therefore, the contribution of stromal subsets in the small intestine would be highly relevant in determining the exact relationship between IL-33, stromal cells, and eosinophils as well as their well-known role in tissue repair. Lastly, how well murine stromal cell biology, in terms of eosinophils and IL-33, reflects that of humans remains to be determined, considering that both are predominant in various type 2-associated pathologies.

STAR★METHODS

Detailed methods are provided in the online version of this paper and include the following:

- KEY RESOURCES TABLE
- RESOURCE AVAILABILITY
  - Lead contact
  - Materials availability
  - Data and code availability
- EXPERIMENTAL MODEL AND STUDY PARTICIPANT DETAILS
  - Mice, helminth infection, treatments, and ethical statement
- METHOD DETAILS
  - Bone marrow chimera
  - Flow cytometry
  - Histology, immunofluorescence microscopy and image quantification
  - Deep tissue imaging of mLN to visualize eosinophils
  - Eosinophil-stromal cell co-culture
  - Eosinophil survival assay
  - RNA isolation and qRT-PCR analysis
  - Bulk RNA sequencing and analysis
  - STRING analysis
- QUANTIFICATION AND STATISTICAL ANALYSIS
  - Statistical analysis

REFERENCES

1. Bajénoff, M., Egen, J.G., Koo, L.Y., Laugier, J.P., Brau, F., Glaichenhaus, N., and Germain, R.N. (2006). Stromal Cell Networks Regulate Lymphocyte Entry, Migration, and Territoriality in Lymph Nodes. Immunity 25, 989–1001. https://doi.org/10.1016/j.immuni.2006.10.011.

2. Lütge, M., De Martin, A., Gil-Cruz, C., Perez-Shibayama, C., Stanossek, Y., Onder, L., Cheng, H.-W., Kurz, L., Cadosch, N., Soneson, C., et al. (2023). Conserved stromal–immune cell circuits secure B cell homeostasis and function. Nat. Immunol. 24, 1149–1160. https://doi.org/10.1038/s41590-023-01503-3.

3. Cremasco, V., Woodruff, M.C., Onder, L., Cupovic, J., Nieves-Bonilla, J.M., Schildberg, F.A., Chang, J., Cremasco, F., Harvey, C.J., Wucherpfennig, K., et al. (2014). B cell homeostasis and follicle confines are governed by fibroblastic reticular cells. Nat. Immunol. 15, 973–981. https://doi.org/10.1038/ni.2965. http://www.nature.com/ni/journal/v15/n10/abs/ni.2965.html#supplementary-information.

4. Link, A., Vogt, T.K., Favre, S., Britschgi, M.R., Acha-Orbea, H., Hinz, B., Cyster, J.G., and Luther, S.A. (2007). Fibroblastic reticular cells in lymph nodes

regulate the homeostasis of naive T cells. Nat. Immunol. *8*, 1255–1265. http://www.nature.com/ni/journal/v8/n11/suppinfo/ni1513_S1.html.

5. De Martin, A., Stanossek, Y., Pikor, N.B., and Ludewig, B. (2024). Protective fibroblastic niches in secondary lymphoid organs. J. Exp. Med. *221*, e20221220. https://doi.org/10.1084/jem.20221220.

6. Hampton, H.R., Bailey, J., Tomura, M., Brink, R., and Chtanova, T. (2015). Microbe-dependent lymphatic migration of neutrophils modulates lymphocyte proliferation in lymph nodes. Nat. Commun. *6*, 7139. https://doi.org/10.1038/ncomms8139.

7. Hampton, H.R., and Chtanova, T. (2016). The lymph node neutrophil. Semin. Immunol. *28*, 129–136. https://doi.org/10.1016/j.smim.2016.03.008.

8. Rothenberg, M.E., and Hogan, S.P. (2006). THE EOSINOPHIL. Annu. Rev. Immunol. *24*, 147–174. https://doi.org/10.1146/annurev.immunol.24.021605.090720.

9. Gurtner, A., Crepaz, D., and Arnold, I.C. (2023). Emerging functions of tissue-resident eosinophils. J. Exp. Med. *220*, e20221435. https://doi.org/10.1084/jem.20221435.

10. Huang, L., and Appleton, J.A. (2016). Eosinophils in Helminth Infection: Defenders and Dupes. Trends Parasitol. *32*, 798–807. https://doi.org/10.1016/j.pt.2016.05.004.

11. Falcone, F.H., Loke, P., Zang, X., MacDonald, A.S., Maizels, R.M., and Allen, J.E. (2001). A Brugia malayi Homolog of Macrophage Migration Inhibitory Factor Reveals an Important Link Between Macrophages and Eosinophil Recruitment During Nematode Infection. J. Immunol. *167*, 5348–5354. https://doi.org/10.4049/jimmunol.167.9.5348.

12. Strandmark, J., Steinfelder, S., Berek, C., Kühl, A.A., Rausch, S., and Hartmann, S. (2017). Eosinophils are required to suppress Th2 responses in Peyer's patches during intestinal infection by nematodes. Mucosal Immunol. *10*, 661–672. https://doi.org/10.1038/mi.2016.93.

13. Voehringer, D., Shinkai, K., and Locksley, R.M. (2004). Type 2 Immunity Reflects Orchestrated Recruitment of Cells Committed to IL-4 Production. Immunity *20*, 267–277. https://doi.org/10.1016/S1074-7613(04)00026-3.

14. Chu, V.T., and Berek, C. (2012). Immunization induces activation of bone marrow eosinophils required for plasma cell survival. Eur. J. Immunol. *42*, 130–137. https://doi.org/10.1002/eji.201141953.

15. Chu, V.T., Beller, A., Rausch, S., Strandmark, J., Zänker, M., Arbach, O., Kruglov, A., and Berek, C. (2014). Eosinophils Promote Generation and Maintenance of Immunoglobulin-A-Expressing Plasma Cells and Contribute to Gut Immune Homeostasis. Immunity *40*, 582–593. https://doi.org/10.1016/j.immuni.2014.02.014.

16. Gurtner, A., Borrelli, C., Gonzalez-Perez, I., Bach, K., Acar, I.E., Núñez, N.G., Crepaz, D., Handler, K., Vu, V.P., Lafzi, A., et al. (2023). Active eosinophils regulate host defence and immune responses in colitis. Nature *615*, 151–157. https://doi.org/10.1038/s41586-022-05628-7.

17. Dubey, L.K., Lebon, L., Mosconi, I., Yang, C.-Y., Scandella, E., Ludewig, B., Luther, S.A., and Harris, N.L. (2016). Lymphotoxin-Dependent B Cell-FRC Crosstalk Promotes De Novo Follicle Formation and Antibody Production following Intestinal Helminth Infection. Cell Rep. *15*, 1527–1541. https://doi.org/10.1016/j.celrep.2016.04.023.

18. Zaiss, M.M., Rapin, A., Lebon, L., Dubey, L.K., Mosconi, I., Sarter, K., Piersigilli, A., Menin, L., Walker, A.W., Rougemont, J., et al. (2015). The Intestinal Microbiota Contributes to the Ability of Helminths to Modulate Allergic Inflammation. Immunity *43*, 998–1010. https://doi.org/10.1016/j.immuni.2015.09.012.

19. Dubey, L.K., Ludewig, B., Luther, S.A., and Harris, N.L. (2019). IL-4Rα-Expressing B Cells Are Required for CXCL13 Production by Fibroblastic Reticular Cells. Cell Rep. *27*, 2442–2458. https://doi.org/10.1016/j.celrep.2019.04.079.

20. Allen, J.E., and Maizels, R.M. (2011). Diversity and dialogue in immunity to helminths. Nat. Rev. Immunol. *11*, 375–388.

21. Mosconi, I., Dubey, L.K., Volpe, B., Esser-von Bieren, J., Zaiss, M.M., Lebon, L., Massacand, J.C., and Harris, N.L. (2015). Parasite Proximity

22. Nussbaum, J.C., Van Dyken, S.J., von Moltke, J., Cheng, L.E., Mohapatra, A., Molofsky, A.B., Thornton, E.E., Krummel, M.F., Chawla, A., Liang, H.-E., and Locksley, R.M. (2013). Type 2 innate lymphoid cells control eosinophil homeostasis. Nature *502*, 245–248. https://doi.org/10.1038/nature12526.

23. Fulkerson, P.C., and Rothenberg, M.E. (2013). Targeting eosinophils in allergy, inflammation and beyond. Nat. Rev. Drug Discov. *12*, 117–129. https://doi.org/10.1038/nrd3838.

24. Dubey, L.K., Karempudi, P., Luther, S.A., Ludewig, B., and Harris, N.L. (2017). Interactions between fibroblastic reticular cells and B cells promote mesenteric lymph node lymphangiogenesis. Nat. Commun. *8*, 367. https://doi.org/10.1038/s41467-017-00504-9.

25. Sinha, R.K., Park, C., Hwang, I.-Y., Davis, M.D., and Kehrl, J.H. (2009). B Lymphocytes Exit Lymph Nodes through Cortical Lymphatic Sinusoids by a Mechanism Independent of Sphingosine-1-Phosphate-Mediated Chemotaxis. Immunity *30*, 434–446. https://doi.org/10.1016/j.immuni.2008.12.018.

26. Chu, V.T., Fröhlich, A., Steinhauser, G., Scheel, T., Roch, T., Fillatreau, S., Lee, J.J., Löhning, M., and Berek, C. (2011). Eosinophils are required for the maintenance of plasma cells in the bone marrow. Nat. Immunol. *12*, 151–159. http://www.nature.com/ni/journal/v12/n2/abs/ni.1981.html#supplementary-information.

27. Fooksman, D.R., Schwickert, T.A., Victora, G.D., Dustin, M.L., Nussenzweig, M.C., and Skokos, D. (2010). Development and Migration of Plasma Cells in the Mouse Lymph Node. Immunity *33*, 118–127. https://doi.org/10.1016/j.immuni.2010.06.015.

28. McCoy, K.D., Stoel, M., Stettler, R., Merky, P., Fink, K., Senn, B.M., Schaer, C., Massacand, J., Odermatt, B., Oettgen, H.C., et al. (2008). Polyclonal and Specific Antibodies Mediate Protective Immunity against Enteric Helminth Infection. Cell Host Microbe *4*, 362–373. https://doi.org/10.1016/j.chom.2008.08.014.

29. Leon, B., Ballesteros-Tato, A., Browning, J.L., Dunn, R., Randall, T.D., and Lund, F.E. (2012). Regulation of TH2 development by CXCR5+ dendritic cells and lymphotoxin-expressing B cells. Nat. Immunol. *13*, 681–690. http://www.nature.com/ni/journal/v13/n7/abs/ni.2309.html#supplementary-information.

30. Katakai, T., Hara, T., Sugai, M., Gonda, H., and Shimizu, A. (2004). Lymph Node Fibroblastic Reticular Cells Construct the Stromal Reticulum via Contact with Lymphocytes. J. Exp. Med. *200*, 783–795. https://doi.org/10.1084/jem.20040254.

31. Suzukawa, M., Koketsu, R., Iikura, M., Nakae, S., Matsumoto, K., Nagase, H., Saito, H., Matsushima, K., Ohta, K., Yamamoto, K., and Yamaguchi, M. (2008). Interleukin-33 enhances adhesion. Lab. Invest. *88*, 1245–1253. https://doi.org/10.1038/labinvest.2008.82.

32. Johnston, L.K., and Bryce, P.J. (2017). Understanding Interleukin 33 and Its Roles in Eosinophil Development. Front. Med. *4*, 51. https://doi.org/10.3389/fmed.2017.00051.

33. Vondenhoff, M.F., Greuter, M., Goverse, G., Elewaut, D., Dewint, P., Ware, C.F., Hoorweg, K., Kraal, G., and Mebius, R.E. (2009). LTβR Signaling Induces Cytokine Expression and Up-Regulates Lymphangiogenic Factors in Lymph Node Anlagen. J. Immunol. *182*, 5439–5445. https://doi.org/10.4049/jimmunol.0801165.

34. Bouffi, C., Rochman, M., Zust, C.B., Stucke, E.M., Kartashov, A., Fulkerson, P.C., Barski, A., and Rothenberg, M.E. (2013). IL-33 Markedly Activates Murine Eosinophils by an NF-κB–Dependent Mechanism Differentially Dependent upon an IL-4–Driven Autoinflammatory Loop. J. Immunol. *191*, 4317–4325. https://doi.org/10.4049/jimmunol.1301465.

35. Feistritzer, C., Kaneider, N.C., Sturn, D.H., Mosheimer, B.A., Kähler, C.M., and Wiedermann, C.J. (2004). Expression and Function of the Vascular Endothelial Growth Factor Receptor FLT-1 in Human Eosinophils. Am. J.

Respir. Cell Mol. Biol. *30*, 729–735. https://doi.org/10.1165/rcmb.2003-0314OC.

36. Chai, Q., Onder, L., Scandella, E., Gil-Cruz, C., Perez-Shibayama, C., Cupovic, J., Danuser, R., Sparwasser, T., Luther, S.A., Thiel, V., et al. (2013). Maturation of Lymph Node Fibroblastic Reticular Cells from Myofibroblastic Precursors Is Critical for Antiviral Immunity. Immunity *38*, 1013–1024. https://doi.org/10.1016/j.immuni.2013.03.012.

37. Yu, C., Cantor, A.B., Yang, H., Browne, C., Wells, R.A., Fujiwara, Y., and Orkin, S.H. (2002). Targeted Deletion of a High-Affinity GATA-binding Site in the GATA-1 Promoter Leads to Selective Loss of the Eosinophil Lineage In Vivo. J. Exp. Med. *195*, 1387–1395. https://doi.org/10.1084/jem.20020656.

38. Lukacs-Kornek, V., Malhotra, D., Fletcher, A.L., Acton, S.E., Elpek, K.G., Tayalia, P., Collier, A.-r., and Turley, S.J. (2011). Regulated release of nitric oxide by nonhematopoietic stroma controls expansion of the activated T cell pool in lymph nodes. Nat. Immunol. *12*, 1096–1104. http://www.nature.com/ni/journal/v12/n11/abs/ni.2112.html#supplementary-information.

39. Schmitz, J., Owyang, A., Oldham, E., Song, Y., Murphy, E., McClanahan, T.K., Zurawski, G., Moshrefi, M., Qin, J., Li, X., et al. (2005). IL-33, an Interleukin-1-like Cytokine that Signals via the IL-1 Receptor-Related Protein ST2 and Induces T Helper Type 2-Associated Cytokines. Immunity *23*, 479–490. https://doi.org/10.1016/j.immuni.2005.09.015.

40. Kannan, Y., Entwistle, L.J., Pelly, V.S., Perez-Lloret, J., Walker, A.W., Ley, S.C., and Wilson, M.S. (2017). TPL-2 restricts Ccl24-dependent immunity to Heligmosomoides polygyrus. PLoS Pathog. *13*, e1006536. https://doi.org/10.1371/journal.ppat.1006536.

41. Grisaru-Tal, S., Rothenberg, M.E., and Munitz, A. (2022). Eosinophil–lymphocyte interactions in the tumor microenvironment and cancer immunotherapy. Nat. Immunol. *23*, 1309–1316. https://doi.org/10.1038/s41590-022-01291-2.

42. Cosway, E.J., White, A.J., Parnell, S.M., Schweighoffer, E., Jolin, H.E., Bacon, A., Rodewald, H.-R., Tybulewicz, V., McKenzie, A.N.J., Jenkinson, W.E., and Anderson, G. (2022). Eosinophils are an essential element of a type 2 immune axis that controls thymus regeneration. Sci. Immunol. *7*, eabn3286. https://doi.org/10.1126/sciimmunol.abn3286.

43. Kumar, V., Dasoveanu, D.C., Chyou, S., Tzeng, T.-C., Rozo, C., Liang, Y., Stohl, W., Fu, Y.-X., Ruddle, N.H., and Lu, T.T. (2015). A Dendritic-Cell-Stromal Axis Maintains Immune Responses in Lymph Nodes. Immunity *42*, 719–730. https://doi.org/10.1016/j.immuni.2015.03.015.

44. Cortes-Selva, D., Ready, A., Gibbs, L., Rajwa, B., and Fairfax, K.C. (2019). IL-4 promotes stromal cell expansion and is critical for development of a type-2, but not a type 1 immune response. Eur. J. Immunol. *49*, 428–442. https://doi.org/10.1002/eji.201847789.

45. Li, C., Ward, L.A., Nguyen, A., Lam, E., Dasoveanu, D., Ahmed, M., Haniuda, K., Buechler, M.B., He, H.H., Ludewig, B., et al. (2022). Neonatal LTβR signaling is required for the accumulation of eosinophils in the inflamed adult mesenteric lymph node. Mucosal Immunol. *15*, 418–427. https://doi.org/10.1038/s41385-022-00493-z.

46. Svensson, M., Bell, L., Little, M.C., DeSchoolmeester, M., Locksley, R.M., and Else, K.J. (2011). Accumulation of eosinophils in intestine-draining mesenteric lymph nodes occurs after Trichuris muris infection. Parasite Immunol. *33*, 1–11. https://doi.org/10.1111/j.1365-3024.2010.01246.x.

47. Hewitson, J.P., Filbey, K.J., Esser-von Bieren, J., Camberis, M., Schwartz, C., Murray, J., Reynolds, L.A., Blair, N., Robertson, E., Harcus, Y., et al. (2015). Concerted Activity of IgG1 Antibodies and IL-4/IL-25-Dependent Effector Cells Trap Helminth Larvae in the Tissues following Vaccination with Defined Secreted Antigens, Providing Sterile Immunity to Challenge Infection. PLoS Pathog. *11*, e1004676. https://doi.org/10.1371/journal.ppat.1004676.

48. Gerner, M.Y., Torabi-Parizi, P., and Germain, R.N. (2015). Strategically Localized Dendritic Cells Promote Rapid T Cell Responses to Lymph-Borne Particulate Antigens. Immunity *42*, 172–185. https://doi.org/10.1016/j.immuni.2014.12.024.

49. Harris, D.P., Goodrich, S., Mohrs, K., Mohrs, M., and Lund, F.E. (2005). Cutting Edge: The Development of IL-4-Producing B Cells (B Effector 2 Cells) Is Controlled by IL-4, IL-4 Receptor α, and Th2 Cells1. J. Immunol. *175*, 7103–7107. https://doi.org/10.4049/jimmunol.175.11.7103.

50. Rana, B.M.J., Jou, E., Barlow, J.L., Rodriguez-Rodriguez, N., Walker, J.A., Knox, C., Jolin, H.E., Hardman, C.S., Sivasubramaniam, M., Szeto, A., et al. (2019). A stromal cell niche sustains ILC2-mediated type-2 conditioning in adipose tissue. J. Exp. Med. *216*, 1999–2009. https://doi.org/10.1084/jem.20190689.

51. Lee, S.H., Chaves, M.M., Kamenyeva, O., Gazzinelli-Guimaraes, P.H., Kang, B., Pessenda, G., Passelli, K., Tacchini-Cottier, F., Kabat, J., Jacobsen, E.A., et al. (2020). M2-like, dermal macrophages are maintained via IL-4/CCL24–mediated cooperative interaction with eosinophils in cutaneous leishmaniasis. Science Immunology *5*, eaaz4415. https://doi.org/10.1126/sciimmunol.aaz4415.

52. Savetsky, I.L., Ghanta, S., Gardenier, J.C., Torrisi, J.S., García Nores, G.D., Hespe, G.E., Nitti, M.D., Kataru, R.P., and Mehrara, B.J. (2015). Th2 Cytokines Inhibit Lymphangiogenesis. PLoS One *10*, e0126908. https://doi.org/10.1371/journal.pone.0126908.

53. Grisaru-Tal, S., Itan, M., Klion, A.D., and Munitz, A. (2020). A new dawn for eosinophils in the tumour microenvironment. Nat. Rev. Cancer *20*, 594–607. https://doi.org/10.1038/s41568-020-0283-9.

54. Travers, J., Rochman, M., Miracle, C.E., Habel, J.E., Brusilovsky, M., Caldwell, J.M., Rymer, J.K., and Rothenberg, M.E. (2018). Chromatin regulates IL-33 release and extracellular cytokine activity. Nat. Commun. *9*, 3244. https://doi.org/10.1038/s41467-018-05485-x.

55. Chen, W., Chen, S., Yan, C., Zhang, Y., Zhang, R., Chen, M., Zhong, S., Fan, W., Zhu, S., Zhang, D., et al. (2022). Allergen protease-activated stress granule assembly and gasdermin D fragmentation control interleukin-33 secretion. Nat. Immunol. *23*, 1021–1030. https://doi.org/10.1038/s41590-022-01255-6.

56. Mackley, E.C., Houston, S., Marriott, C.L., Halford, E.E., Lucas, B., Cerovic, V., Filbey, K.J., Maizels, R.M., Hepworth, M.R., Sonnenberg, G.F., et al. (2015). CCR7-dependent trafficking of RORγ+ ILCs creates a unique microenvironment within mucosal draining lymph nodes. Nat. Commun. *6*, 5862. https://doi.org/10.1038/ncomms6862. https://www.nature.com/articles/ncomms6862#supplementary-information.

57. Akuthota, P., Ueki, S., Estanislau, J., and Weller, P.F. (2013). Human Eosinophils Express Functional CCR7. Am. J. Respir. Cell Mol. Biol. *48*, 758–764. https://doi.org/10.1165/rcmb.2012-0499OC.

58. Shi, H.-Z., Humbles, A., Gerard, C., Jin, Z., and Weller, P.F. (2000). Lymph node trafficking and antigen presentation by endobronchial eosinophils. J. Clin. Invest. *105*, 945–953. https://doi.org/10.1172/JCI8945.

59. Chow, J.Y.S., Wong, C.K., Cheung, P.F.Y., and Lam, C.W.K. (2010). Intracellular signaling mechanisms regulating the activation of human eosinophils by the novel Th2 cytokine IL-33: implications for allergic inflammation. Cell. Mol. Immunol. *7*, 26–34. https://doi.org/10.1038/cmi.2009.106.

60. Carrasco, Y.R., Fleire, S.J., Cameron, T., Dustin, M.L., and Batista, F.D. (2004). LFA-1/ICAM-1 Interaction Lowers the Threshold of B Cell Activation by Facilitating B Cell Adhesion and Synapse Formation. Immunity *20*, 589–599. https://doi.org/10.1016/S1074-7613(04)00105-0.

61. Langston, W., Chidlow, J.H., Jr., Booth, B.A., Barlow, S.C., Lefer, D.J., Patel, R.P., and Kevil, C.G. (2007). Regulation of endothelial glutathione by ICAM-1 governs VEGF-A-mediated eNOS activity and angiogenesis. Free Radic. Biol. Med. *42*, 720–729. https://doi.org/10.1016/j.freeradbiomed.2006.12.010.

62. Cherry, W.B., Yoon, J., Bartemes, K.R., Iijima, K., and Kita, H. (2008). A novel IL-1 family cytokine, IL-33, potently activates human eosinophils. J. Allergy Clin. Immunol. *121*, 1484–1490. https://doi.org/10.1016/j.jaci.2008.04.005.

63. Angulo, E.L., McKernan, E.M., Fichtinger, P.S., and Mathur, S.K. (2019). Comparison of IL-33 and IL-5 family mediated activation of human eosinophils. PLoS One *14*, e0217807. https://doi.org/10.1371/journal.pone.0217807.

64. Jung, Y., Wen, T., Mingler, M.K., Caldwell, J.M., Wang, Y.H., Chaplin, D.D., Lee, E.H., Jang, M.H., Woo, S.Y., Seoh, J.Y., et al. (2015). IL-1β in eosinophil-mediated small intestinal homeostasis and IgA production. Mucosal Immunol. *8*, 930–942. https://doi.org/10.1038/mi.2014.123.

65. Spencer, L.A., Melo, R.C.N., Perez, S.A.C., Bafford, S.P., Dvorak, A.M., and Weller, P.F. (2006). Cytokine receptor-mediated trafficking of pre-formed IL-4 in eosinophils identifies an innate immune mechanism of cyto-kine secretion. Proc. Natl. Acad. Sci. USA *103*, 3333–3338. https://doi.org/10.1073/pnas.0508946103.

66. Sabin, E.A., Kopf, M.A., and Pearce, E.J. (1996). Schistosoma mansoni egg-induced early IL-4 production is dependent upon IL-5 and eosino-phils. J. Exp. Med. *184*, 1871–1878. https://doi.org/10.1084/jem.184.5.1871.

67. Fabre, V., Beiting, D.P., Bliss, S.K., Gebreselassie, N.G., Gagliardo, L.F., Lee, N.A., Lee, J.J., and Appleton, J.A. (2009). Eosinophil Deficiency Com-promises Parasite Survival in Chronic Nematode Infection1. J. Immunol. *182*, 1577–1583. https://doi.org/10.4049/jimmunol.182.3.1577.

68. Ignacio, A., Shah, K., Bernier-Latmani, J., Köller, Y., Coakley, G., Moyat, M., Hamelin, R., Armand, F., Wong, N.C., Ramay, H., et al. (2022). Small intestinal resident eosinophils maintain gut homeostasis following micro-bial colonization. Immunity *55*, 1250–1267.e12. https://doi.org/10.1016/J.IMMUNI.2022.05.014.

69. Cui, A., Huang, T., Li, S., Ma, A., Pérez, J.L., Sander, C., Keskin, D.B., Wu, C.J., Fraenkel, E., and Hacohen, N. (2024). Dictionary of immune re-sponses to cytokines at single-cell resolution. Nature *625*, 377–384. https://doi.org/10.1038/s41586-023-06816-9.

70. Neill, D.R., Wong, S.H., Bellosi, A., Flynn, R.J., Daly, M., Langford, T.K.A., Bucks, C., Kane, C.M., Fallon, P.G., Pannell, R., et al. (2010). Nuocytes represent a new innate effector leukocyte that mediates type-2 immunity. Nature *464*, 1367–1370. https://doi.org/10.1038/nature08900.

71. Yang, C.-Y., Vogt, T.K., Favre, S., Scarpellino, L., Huang, H.-Y., Tacchini-Cottier, F., and Luther, S.A. (2014). Trapping of naive lymphocytes triggers rapid growth and remodeling of the fibroblast network in reactive murine lymph nodes. Proc. Natl. Acad. Sci. USA *111*, E109–E118. https://doi.org/10.1073/pnas.1312585111.

STAR★METHODS

KEY RESOURCES TABLE

REAGENT or RESOURCE	SOURCE	IDENTIFIER
Antibodies		
Anti-mouse B220	BioLegend	Cat No.# 103226; RRID:AB_389330
Anti-mouse CD11b	Invitrogen	Cat No.# 63-0112-82; RRID:AB_2637408
Anti-mouse CD11b	BioLegend	Cat No.#101212; RRID:AB_312795
Anti-mouse CD11b	BD Biosciences	Cat No.# 553310; RRID:AB_394774
Anti-mouse CD11b	BioLegend	Cat No.# 101241; RRID:AB_11218791
Anti-mouse CD11c	BioLegend	Cat No.# 117324; RRID:AB_830649
Anti-mouse CD11c	BioLegend	Cat No.#117310; RRID:AB_313779
Anti-mouse CD11c	Invitrogen	Cat No.# 47-0114-82; RRID:AB_1548652
Anti-mouse CD19	BioLegend	Cat No.# 152412
Anti-mouse CD19	BioLegend	Cat No.# 152410; RRID:AB_2629839
Anti-mouse CD19	BD Biosciences	Cat No.# 563557; RRID:AB_2722495
Anti-mouse CD3	BioLegend	Cat No.# 100210; RRID:389301
Anti-mouse CD3	Invitrogen	Cat No.# 45-0031-82; RRID:1107000
Anti-mouse CD45	BioLegend	Cat No.# 103112; RRID:AB_312977
Anti-mouse CD45	BD Biosciences	Cat No.# 536410
Anti-mouse CD5	Invitrogen	Cat No.# 45-0051-82; RRID:AB_914334
Anti-mouse FCƐR1	Invitrogen	Cat No.# 17-5898-82; RRID:AB_10718824
Anti-mouse I-A/I-E	BioLegend	Cat No.# 107622; RRID:AB_493728
Anti-mouse IgD	BioLegend	Cat No.#405718; RRID:AB_10730619
Anti-mouse IgM	BioLegend	Cat No.# 406508; RRID:AB_315058
Anti-mouse Ly-6C	BioLegend	Cat No.# 128044; RRID:AB_2566577
Anti-mouse Ly-6G	BioLegend	Cat No.# 127617; RRID:AB_1877262
Anti-mouse MHC II	Invitrogen	Cat No.# 48-5321-82; RRID:AB_1272204
Anti-mouse Siglec-F	Invitrogen	Cat No.# 61-1702-80; RRID:AB_2815311
Anti-mouse Siglec-F	Invitrogen	Cat No.# 53-1702-82; RRID:AB_2784747
Anti-mouse Siglec-F	BD Biosciences	Cat No. # 552126; RRID:AB_39431
Anti-mouse Siglec-F	BD Biosciences	Cat No.# 740388; RRID:AB_2740118
Anti-mouse Siglec-F	BioLegend	Cat No.# 155508; RRID:AB_2750237
Anti-muse I-A/I-E	BioLegend	Cat No.# 107616; RRID:AB_493523
Biotin anti-mouse B220	BioLegend	Cat No.# 103204; RRID:AB_312989
Purified anti-mouse CD16/32	BioLegend	Cat No.# 101302; RRID:AB_312801
Rabbit anti-mouse CCL24	Bioss Antibodies	Cat No.# bs-2483R; RRID:AB_10856953
Biotin anti-mouse CD138 (Clone 281-2)	BD Biosciences	Cat No.# 553713; RRID:AB_394999
Rat anti-mouse ER-TR7	BMA Biomedicals	Cat No.#T-2109; RRID:AB_1227372
Goat anti-mouse IL-33	R&D Systems	Cat No.# AF3626; RRID:AB_884269
Rabbit anti-mouse Lyve1	ReliaTech	Cat No.# 103-PA50; RRID:AB_2783787
Rat anti-mouse GP-38/Podoplanin	Abcam	Cat No.# ab256559; RRID:AB_2936436
Syrian hamster anti-mouse GP-38	Hybridoma (clone 8.1.1)	N/A
Rat anti-mouse Siglec-F (Clone: 1RNM44N)	eBioscience	Cat No.# 14-1702-82; RRID:AB_2572866
Donkey anti-goat Alexa 488	Jackson Immunoresearch	Cat No.# 705-545-003; RRID:AB_2340428
Donkey anti-goat Alexa 647	Jackson Immunoresearch	Cat No.# 705-607-003; RRID:AB_2340439
Donkey anti-rabbit Alexa 568	Invitrogen	Cat No.# A10042; RRID:AB_2534017
Donkey anti-rabbit Alexa 647	Invitrogen	Cat No.# A31573; RRID:AB_2536183

(Continued on next page)

Continued

REAGENT or RESOURCE	SOURCE	IDENTIFIER
Donkey anti-rabbit Alexa 488	Invitrogen	Cat No.# A21206; RRID:AB_2535792
Donkey anti-rat Alexa 488	Invitrogen	Cat No.# A21208; RRID:AB_141709
Donkey anti-rat Alexa 647	Invitrogen	Cat No.# A48272; RRID:AB_2893138
Donkey anti-rat IgG-Alexa 647	Jackson Immunoresearch	Cat No# 712-605-150; RRID:AB_2340693
Goat anti-rat IgG-Alexa 568	Thermo Fischer	Cat No# A11077; RRID:AB_2534121
Goat anti-Syrian hamster IgG-Alexa 488	Jackson Immunoresearch	Cat No# 107-545-142; RRID:AB_2337478
Goat anti-Syrian hamster IgG-Alexa 647	Jackson Immunoresearch	Cat No# 107-606-142; RRID:AB_2337483
Horse anti-rabbit ImmPRESS HRP	Vector Laboratories	Cat No.# MP-7401; RRID:AB_2336529
Horse anti-rat ImmPRESS HRP	Vector Laboratories	Cat No.# MP-7444; RRID:AB_3148621
Rabbit anti-Syrian hamster IgG-Alexa 647	Jackson Immunoresearch	Cat No# 307-605-003; RRID:AB_2339601
Anti-IL-4 antibody (Clone:11B11)	Bio X Cell	Cat No.# BE0045; RRID:AB_1107707
Anti-LTβR antibody (Clone:4H8WH2)	Adipogen	Cat No.# AG-20B-0008-C100
Normal Goat IgG Control	R&D systems	Cat No#. AB-108-C; RRID:AB_354267
Normal Rabbit IgG Control	R&D systems	Cat No#. AB-105-C; RRID:AB_354266
Biological samples		
Normal mouse serum	Naive mouse (C57BL/6)	N/A
Normal donkey serum	Millipore	S30-100 mL
Chemicals, peptides and recombinant proteins		
Paraformaldehyde	Merk-Millipore	Cat No.# 104005
Collagenase P	Roche	Cat No.# 11215809103
Dispase	Roche	Cat No.# 04942078001
DNase I	Roche	Cat No.# 11284932001
Ethylenediamine tetraacetic acid (EDTA)	Applichem	Cat No.# A4892
Protease Inhibitor Cocktail	Roche	Cat No.#11873580001
Trypsin	Promega	Cat No.#V5280
RPMI 1640 Medium	Gibco	Cat No.# 11875093
Fetal Bovine Serum	Sigma	Cat No.#F0926
Bovine Serum Albumin	Sigma	Cat No.# A7030-500G
Liberase-TL Research Grade	Roche	Cat No.# 5401020001
Triton X-100	Sigma	Cat No.#T8787
Murine Recombinant Stem Cell Factor	PeproTech	Cat No.# 250-03
Murine Recombinant FLT-3 Ligand	PeproTech	Cat No.# 250-31L
Murine Recombinant IL-5	PeproTech	Cat No.# 215-15
Murine Recombinant IL-4	PeproTech	Cat #214-14
DAPI	Sigma Aldrich	Cat No.#D9542
Aqua (Live/Dead)	Life Technologies	Cat No.#L34966A
Fixable Viability Stain 780	BD Biosciences	Cat No.# 565388
Strepavidin Alexa 488	Molecular Probes	Cat No.# S-11223
Strepavidin Alexa 488	Invitrogen	Cat No.#S11223
Streptavidin Alexa 568	Molecular Probes	Cat No.# S-11226
Streptavidin Alexa 568	Molecular Probes	Cat No.# S-21374
Streptavidin Alexa 568	Invitrogen	Cat No.#S11226
Streptavidin 647	Molecular Probes	Cat No.# S-21374
Streptavidin 647	Invitrogen	Cat No.#S32357
Streptavidin HRP	Jackson Immunoresearch	Cat No.# 016-030-084
Streptavidin APC	BioLegend	Cat No.# 405207
Streptavidin PE-Texas red	BD Biosciences	Cat No.# 551487
ProLong™Gold Antifade Mountant	ThermoFischer	Cat No.#P36934

Continued

REAGENT or RESOURCE	SOURCE	IDENTIFIER
Tyramide signal amplification kit (Alexa 488 and Alexa 568)	ThermoFischer	Cat No.#T20932/34
Tissue-Tek Optimum Cutting Temperature Compound (OCT)	Fischer Scientific	Cat No.# 14-373-65
Acetone for HPLC, ≥99.9%	Sigma Aldrich	Cat No.# 270725
Critical commercial assays		
Light Cycler 480 SYBR Green I Master Mix	Roche	Cat No.# 04707516001
PowerUp SYBR Green Master Mix	Applied Biosystems	Cat No.# A25778
FastStart Universal SYBR Green Master (Rox)	Roche	Cat No.# 04913914001
Murine depleting anti-CD45 microbeads	Miltenyi Biotec	Cat No.# 130-052-301
Murine B cell Isolation Kit	Miltenyi Biotec	Cat No.# 130-090-862
Murine anti-SiglecF Microbeads	Miltenyi Biotec	Cat No.# 130-118-513
MACS Clearing Kit	Miltenyi Biotec	Cat No.# 130-126-719
Direct-zol RNA MiniPrep Kit	Zymo Research	Cat No.#R2051
RNeasy Mini Kit	Qiagen	Cat No.# 74106
Revert Aid First Strand cDNA Synthesis Kit	ThermoFischer	Cat No.#K1622
High-Capacity cDNA Reverse Transcription Kit	Applied Biosystems	Cat No.# 4368814
M-MLV Buffer Pack	Promega	Cat No.#M5313
M-MLV Reverse Transcriptase	Promega	Cat No.#M1705
RNA Protect Cell Reagent	Qiagen	Cat No.# 76526
Experimental models: Organisms/strains		
Mouse: C57BL/6j (WT)	Charles River/Jackson Laboratory	Strain code: 027; RRID:IMSR_JAX:000664
BALB/c (WT)	In-house breeding	RRID:IMSR_JAX:000651
Mouse: JhT knockout	Ref. Dubey et al.[17]	N/A
Mouse: IL-4Rα knockout	Ref. Dubey et al.[17]	N/A
Mouse: LT-β knockout	Ref. Dubey et al.[17]	N/A
Mouse: TCR-βδ knockout	Ref. Dubey et al.[17]	N/A
Mouse: C57BL/6N-Tg (Ccl19 Cre) (+Ccl19-Cre)	Ref. Chai et al.[36]	N/A
Mouse: *Ltbr*fl/fl	Ref. Dubey et al.[17] and Chai et al.[36]	N/A
Mouse: C.129S1(B6)-Gata1tm6Sho/J (ΔdblGATA)	Jackson Laboratory Ref.[37]	RRID:IMSR_JAX:005653
Mouse: B6(C)-Il5tm1.1(icre)Lky/J (Red5)	Jackson Laboratory	RRID:IMSR_JAX:030926
Mouse: IL-13GFP/GFP	Ref. Neill et al.[70]	Prof Andrew McKenzie
Parasite: *Heligmosomoides Polygyrus*	Ref. Dubey et al.[17]	N/A
Deposited data and publicly available data		
RNA-seq	This manuscript	GSE272167
RNA-seq	Ref. Gurtner et al.[16], and Bouffi et al.[34]	GSE43660, GSE182001
Oligonucleotides		
Ccl5-Fw: CCTCACCATCATCCTCACTGCA	Integrated DNA Technologies	N/A
Ccl5-Rv: TCTTCTCTGGGTTGGCACACAC	Integrated DNA Technologies	N/A
Ccl11-Fw: CCCAACACACTACTGAAGAGCTACAA	Integrated DNA Technologies	N/A
Ccl11-Rv: TTTGCCCAACCTGGTCTTG	Integrated DNA Technologies	N/A
Ccl24-Fw: GCAGCATCTGTCCCAAGG	Integrated DNA Technologies	N/A
Ccl24-Rv: GCAGCTTGGGGGTCAGTACA	Integrated DNA Technologies	N/A
Il33-Fw: CACATTGAGCATCCAAGGAA	Integrated DNA Technologies	N/A
Il33-Rv: ACAGATTGGTCATTGTATGTACTCAG	Integrated DNA Technologies	N/A

(Continued on next page)

Continued

REAGENT or RESOURCE	SOURCE	IDENTIFIER
Vegfa-Fw: GCTGTACCTCCACCATGCCAAG	Integrated DNA Technologies	N/A
Vegfa-Rv: ACTCCAGGGCTTCATCG	Integrated DNA Technologies	N/A
Icam1-Fw: GACAGTACTGTACCACTCTC	Integrated DNA Technologies	N/A
Icam1-Rv: CCTGAGCCTTCTGTAACTTG	Integrated DNA Technologies	N/A
MhcII-Fw: CTCCGAAAGGCATTTCGT	Integrated DNA Technologies	N/A
MhcII-Rv: CTGGCTGTTCCAGTACTC	Integrated DNA Technologies	N/A
Ccr7-Fw: AGAGGCTCAAGACCATGACGGA	Integrated DNA Technologies	N/A
Ccr7-Rv: TCCAGGACTTGGCTTCGCTGTA	Integrated DNA Technologies	N/A
Il6-Fw: GCTACCAAACTGGATATAATCAGGA	Integrated DNA Technologies	N/A
Il6-Rv: CCAGGTAGCTATGG- TACTCCAGAA	Integrated DNA Technologies	N/A
Il1β-Fw: CAGTTGTCTAATGGGAACGTCA	Integrated DNA Technologies	N/A
Il1β-Rv: GCACCTTCTTTTCCTTCATCTTT	Integrated DNA Technologies	N/A
Gapdh-Fw: GTGCCAGCCTCGTCCCG	Integrated DNA Technologies	N/A
Gapdh-Rv: TTGCCGTGAGTGGAGTCA	Integrated DNA Technologies	N/A
β-actin-Fw: CTTTTCACGGTTGGCCTTAG	Integrated DNA Technologies	N/A
β-actin-Rv: CCCTGAAGTACCCCATTGAAC	Integrated DNA Technologies	N/A
Software and algorithms		
BD FACS Diva 8	BD Biosciences	http://www.bdbiosciences.com/us/instruments/research/software/flow-cytometry-acquisition/bd-facsdiva-software/m/111112/overview
FlowJo Versions 10	Tree Star	https://www.flowjo.com/solutions/flowjo/downloads/previous-versions
Zeiss ZEN 2010	Carl Zeiss	https://www.zeiss.com/microscopy/int/products/microscope-software/zen-lite.html
GraphPad Prism 10.0 (V10.2.3)	GraphPad	https://www.graphpad.com/scientific-software/prism/
Imaris Versions 8	Bitplane	http://www.bitplane.com/imaris
Olympus slide scanner software (OlyVIA v.2.6)	Olympus	https://www.olympus-lifescience.com/en/microscopes/virtual/vs120/
3Dhistec Slide Viewer software v2.7	HisTech	https://www.3dhistech.com/
ImageJ software	Open source	ImageJ NIH
VSI reader action bar	EPFL BioImaging & Optics Platform (BIOP)	EPFL BioImaging & Optics Platform (BIOP)
FIJI tools, action bar and analysis	EPFL BioImaging & Optics Platform (BIOP)	EPFL BioImaging & Optics Platform (BIOP)
HALO Quantitative Image Analysis	Indica labs	https://indicalab.com/
BioRender.com	BioRender	https://www.biorender.com/
Dr. Tom Visualization Solution	BGI	https://www.bgi.com/global/service/dr-tom
Immgen.org	ImmGen	https://www.immgen.org/
STRING v12	STRING	https://cn.string-db.org
Other		
Zeiss LSM800 microscope	Zeiss	www.zeiss.com
VS120 Virtual Slide Microscope	Olympus	https://www.olympus-lifescience.com/en/microscopes/virtual/vs120/
3Dhistech Pannoramic250 slide scanner	3Dhistech	https://www.3dhistech.com/
Zeiss LSM 710 with Airy scan	Carl Zeiss	www.zeiss.com

RESOURCE AVAILABILITY

Lead contact
Further information and requests for resources and reagents should be directed to the lead contact, Lalit Kumar Dubey (lalit.dubey@qmul.ac.uk or lalitkumardubey@gmail.com).

Materials availability
This study did not generate new unique reagents. Other materials/mouse lines used in this study are available upon execution of a suitable Materials Transfer Agreement.

Data and code availability
- All relevant data supporting the research findings of this study are available within the paper or provided within the supplementary figures and files. RNA-seq processed data from this study and previous studies used for comparative analysis are accessible via GEO accession number GSE272167, GSE43660, GSE182001.
- This paper does not report original code.
- Any additional information required to reanalyze the data reported in this paper is available from the lead contact upon reasonable request.

EXPERIMENTAL MODEL AND STUDY PARTICIPANT DETAILS

Mice, helminth infection, treatments, and ethical statement
All animal procedures were performed using 7-12-week-old mice (in age and sex-matched groups) in accordance with the institutional Animal Welfare Ethical Review Body (AWERB) and UK Home Office guidelines. All studies were ethically reviewed and approved by an institutional body and carried out under the Animals (Scientific Procedures) Act 1986. C57BL/6J (WT) mice were purchased from Charles River Laboratories. JhT$^{-/-}$, IL-4R$\alpha^{-/-}$, IL-5$^{R5/R5}$ and IL-13$^{gfp/gfp}$ mice[70] were bred on the C57BL/6J background and maintained under specific pathogen-free conditions. IL-4R$\alpha^{-/-}$ and Δ-dblGATA-1 mice (BALB/c background), IL-5$^{Red5/R5}$ and IL-13$^{gfp/gfp}$ mice were housed and maintained at École Polytechnique Fédérale de Lausanne (EPFL), Switzerland (authorization numbers: VD2238.1 and VD3001), and at the University of Manchester, UK. LT-$\beta^{-/-}$ and TCR$\beta\delta^{-/-}$ mice were maintained at the University of Lausanne, Switzerland, and were a kind gift from Sanjiv A. Luther (Lausanne, Switzerland). IL-13$^{gfp/gfp}$ were originally obtained from Andrew N.J. McKenzie (Cambridge, UK). CCL19^{Cre}x LTβR$^{fl/fl}$ mice were provided by Burkhard Ludewig (St. Gallen, Switzerland). All mice were maintained under specific pathogen-free conditions, with water and chow provided *ad libitum*. Throughout the study, mice were orally infected with 200 L3 stage *Heligmosomoides polygyrus* (*Hp*) and were sacrificed at indicated time points to study the mesenteric lymph node (mLN).

METHOD DETAILS

Bone marrow chimera
Bone marrow chimeras were set up as previously described.[24] In brief, bone marrow (BM) was obtained from the femur and tibia of donor mice and injected intravenously into C57BL/6J or IL-4R$\alpha^{-/-}$ recipient mice that had been previously irradiated twice with 450 rad with 4-h intervals between irradiation sessions. All mice were maintained in specific pathogen-free conditions. For the generation of complete BM chimeric mice which lacked IL-4Rα on CD45$^-$ or CD45$^+$ cells, IL-4R$\alpha^{-/-}$ mice received WT-BM or WT mice received IL-4R$\alpha^{-/-}$ BM, respectively. Mice lacking IL-4Rα on B cells and WT chimeras were generated using irradiated WT mice reconstituted with 80% JhT$^{-/-}$ BM and 20% IL-4R$\alpha^{-/-}$ BM or with 80% JhT$^{-/-}$ and 20% WT BM, respectively. For the generation of mice with B cells or T cells lacking lymphotoxin expression (B-Lt$\beta^{-/-}$ or T-Lt$\beta^{-/-}$), C57BL/6J recipient mice were reconstituted with 80% JhT$^{-/-}$ or 80% TCR$\beta\delta^{-/-}$ bone marrow plus 20% Lt$\beta^{-/-}$ bone marrow. Control mice were generated using WT recipient mice which were reconstituted with 80% JhT$^{-/-}$ or 80% TCR$\beta\delta^{-/-}$ bone marrow plus 20% WT bone marrow, respectively. All chimeric mice received an antibiotic in their drinking water for 4–6 weeks following the BM reconstitution and were subjected to infection 8 weeks following reconstitution.

Flow cytometry
At the given experimental time points, mice were killed and the whole mLNs were isolated, and single-cell suspensions were generated using enzymatic digestion. mLNs were incubated at 37°C in digestion medium (RPMI-1640 supplemented with 0.8 mg/mL dispase, 0.2 mg/mL Collagenase P [Roche] and 0.1 mg/mL DNase I [Invitrogen]) and gently pipetted at 5-min intervals to ensure complete dissociation of the tissue. Following digestion, the single-cell suspension was filtered through a 70 μm cell strainer, counted, and resuspended in FACS buffer (PBS supplemented with 2% FBS and 5 mM EDTA). For eosinophil staining, cells were incubated for 30 min with an antibody cocktail and identified as CD45$^+$CD3$^-$CD19$^-$CD11c$^-$Ly6G$^-$CD11b$^+$Siglec-F$^+$ cells (Figure S1). Samples were acquired on the BD machine and analyzed using FlowJo V.10.

Histology, immunofluorescence microscopy and image quantification

The entire mLN chain was carefully dissected, weighed, imaged, and embedded in Tissue-Tek optimum cutting temperature control compound (OCT) and frozen in an ethanol ice bath. Cryostat sections (8 μm in thickness) were cut from a 400 μm span of the mLN onto Superfrost Plus glass slides, air-dried, and fixed for 10–15 min in ice-cold acetone. After rehydration in PBS, sections were blocked with 1% (w/v) BSA and 1–4% (v/v) mouse and donkey serum. Immunofluorescence staining was performed using antibodies (Siglec-F, Pdpn, Lyve1, CD138, etc.). Sections were incubated overnight at 4°C in the primary antibodies. On the following day, sections were washed four times with PBS, and primary antibodies were detected using fluorescently labeled secondary antibodies and nuclei counterstained with DAPI prior to mounting sections using ProLong anti-fade reagents (Life Technologies). Images were acquired on an Olympus VS120−SL full slide scanner using a 20x/0.75 air objective and an OlympusXM10 B/W camera or on a 3Dhistech Pannoramic250 slide scanner using a 20× objective equipped with fluorescence filters for DAPI, FITC, TRITC, and Cy5 with 20x/40× objective. On occasions, LSM710 (20x/1.2 or 40x/1.4 using regular PMTs, 1AU pinhole, Z spacing 1−10μm) laser scanning confocal microscope was used to acquire images for quantification. For quantitative measurements, immunofluorescence images from naive and infected mice mLN were acquired and segmented using an ImageJ/Fiji pipeline. A threshold−based approach was used to measure areas specific for a given marker and expressed as the percentage of total area within the tissue occupied by the given marker. 3Dhistech Pannoramic250 slide scanner images were visualized and processed using 3D-histec Slide Viewer software v2.7. Brightfield and immunofluorescence images (for IL-33, Lyve-1 and CD138) were quantified using Indica Labs Halo platform. Whole lymph nodes, interfollicular regions and lymphatic vessels were analyzed by drawing regions of interest (ROIs). Images were quantified using CytoNuclear module and HighPlex Fl v4.2 module as appropriate. For all analyses DAPI was set as the nuclear stain and was manually checked for nuclear segmentation, size, and stain intensity. The final figure panels (graphs and images) were arranged and converted to.TIF file (LZW compression) using Adobe Photoshop 24.02 edition 2023. Schematic figures and graphical abstract were generated using BioRender.com.

Deep tissue imaging of mLN to visualize eosinophils

C57BL/6J and IL-4R$\alpha^{-/-}$ mice were infected with *Hp* and the mLN was collected at 21 dpi for vibratome sectioning and deep tissue imaging to identify eosinophil association with stromal cells. 200μm thick vibratome sections were generated using Leica VT1200S vibratome. Post sectioning, tissue was blocked in blocking solution followed by two stage staining as described previously with slight modification.[24] We used antibodies against well-established markers like Siglec-F, Lyve1, and GP38 to identify eosinophils, lymphatics, and FRCs, respectively. The stained tissue was cleared using the Miltenyi Biotec MACS Clearing Kit protocol as per the manufacturer's recommendation. Stained samples were imaged using a Zeiss confocal microscope. The 3D reconstruction and movies were made using IMARIS (Bitplane) and exported as a.mpg file.

Eosinophil-stromal cell co-culture

Bone marrow-derived eosinophils were generated *in vitro* as described previously.[42] Briefly, bone marrow cells were obtained from femurs and tibiae of WT C57BL/6 mice by flushing with complete RPMI 1640 media containing 10% heat inactivated fetal bovine serum (FBS) (Sigma-Aldrich, non-USA origin). Red blood cells were lysed using ACK lysis buffer, and 1×10^6 cells/mL were plated in RPMI-1640 medium containing 10% FBS, penicillin-streptomycin and further supplemented with stem cell factor (100 ng/mL), and FLT3Ligand (100 ng/mL) (both from Miltenyi Biotec) from culture days 0–4. Cultures were changed on day 4 to new complete RPMI 1640 medium containing recombinant murine IL-5 (10 ng/mL, Peprotech) and further fed with IL-5 every other day between days 10–14. Cells were collected on day 14 (typically containing more than 92% eosinophils), counted, and used for the co-culture experiment. Naive B cells were isolated from whole mLN by negative selection as described previously.[24] mLN derived stromal cells were cultured *in vitro* as previously described.[38] In brief, single-cell suspensions from whole mLN were generated using enzymatic digestion and plated at a density of 20×10^6 in a 6-well plate. After 24 h non-adherent cells were removed and adherent cells were further cultured for 7–10 days, with culture media changed every other day. After 7–10 days of culture, the adherent cells containing primarily FRCs and LECs were removed and seeded in a 24-well plate at a density of 0.5×10^6 per well. Stromal cells were co-cultured with 1×10^6 naive B cells or stimulated with 2 μg/mL anti-LTβR antibody for 16 h in triplicate wells. The stromal cells were washed thrice with PBS to remove agonist antibody or B cells before adding the eosinophils. After washing 0.5×10^6 eosinophils were added to activated stroma and co-cultured for an additional 8 h. Post co-culture, eosinophils from triplicate wells were pooled and stroma were harvested and stored in RNA lysis buffer at −80°C until analyzed for gene expression and bulk RNA sequencing as detailed below. In a separate set of experiments, FRCs were either stimulated with anti-LTβR agonist antibody (Clone 4H8WH2, 2 μg/ml, Adipogen) or with B cells isolated from mLN using negative selection (1:5 ratio) for 24 h. Post stimulation, cells were washed, and triplicate wells were pooled and stored in RNA lysis buffer at −80°C until analyzed for gene expression.

Eosinophil survival assay

Bone-marrow derived eosinophils and FRCs were generated as previously stated. The stromal subsets were seeded in a 24-well plate at a density of 0.20×10^6 cells/well. Stromal cells were either left unstimulated or primed with anti-LTβR agonist antibody (2 μg/mL) for 16 h. Eosinophils were added to the activated FRCs culture at a ratio of 3:1 (eosinophils: FRCs) and analyzed at 0, 6, 24, 48 and 72 h post initiation of the co-culture. Cells were collected at each time point and stained for Siglec-F and CD11b to identify the eosinophil lineage and DAPI to determine the viability of the cells. Samples were acquired on a BD LSR II- SORP machine and analyzed using FlowJo V.10.

RNA isolation and qRT-PCR analysis

The stromal and cellular fractions were separated as previously described.[38,71] In brief, the mLN was gently mashed through a 40μm cell strainer using a 5 mL syringe plunger. The filtered cells represented the cellular fraction, and the matter left on the strainer represented the stromal cell fraction. The RNA from the stromal fraction was extracted with Direct-zol RNA MiniPrep Kit (Zymo Research) and reverse transcribed using RevertAid cDNA synthesis reagents (Thermo Scientific) for qPCR analysis. mLNs from chimeric mice were washed in RNA Protect Cell Reagent (Qiagen) and the RNA was extracted using the Qiagen Rneasy Mini Kit. RNA from the co-culture experiment was extracted using the Rneasy UCP Micro Kit (Qiagen), and reverse transcribed using a high-capacity cDNA reverse transcription kit (Applied Biosystems). The qPCR was performed using PowerUp SYBR Green Master Mix (Applied Biosystems) on an Applied Biosystems 7900HT system. The following primers were used to detect the various gene expression. *Ccl5-Fw*: CCTCACCATCATCCTCACTGCA, *Ccl5-Rv*: TCTTCTCTGGGTTGGCACACAC; *Ccl11-Fw*: CCCAACACACTACTGAAGAG CTACAA *Ccl11-Rv*: TTTGCCCAACCTGGTCTTG; *Ccl24-Fw*: GCAGCATCTGTCCCAAGG, *Ccl24-Rv*: GCAGCTTGGGGTCAGTACA; *Il33-Fw*: CACATTGAGCATCCAAGGAA; *Il33-Rv*: ACAGATTGGTCATTGTATGTACTCAG; *Vegfa-Fw*: GCTGTACCTCCACCATGC CAAG; *Vegfa-Rv*: ACTCCAGGGCTTCATCG; *Icam1-Fw*: GACAGTACTGTACCACTCTC; *Icam1-Rv*: CCTGAGCCTTCTGTAACTTG; *MhcII-Fw*: CTCCGAAAGGCATTTCGT; *MhcII-Rv*: CTGGCTGTTCCAGTACTC; *Ccr7-Fw*: AGAGGCTCAAGACCATGACGGA; *Ccr7-Rv*: TCCAGGACTTGGCTTCGCTGTA; *Il6-Fw*: GCTACCAAACTGGATATAATCAGGA; *Il6-Rv*: CCAGGTAGCTATGG- TACTCCAGAA; *Il1β-Fw*: CAGTTGTCTAATGGGAACGTCA; *Il1β-Rv*: GCACCTTCTTTTCCTTCATCTTT; *Gapdh-Fw*: GTGCCAGCCTCGTCCCG, *Gapdh-Rv*: TTGCCGTGAGTGGAGTCA; *β-actin-Fw*: CTTTTCACGGTTGGCCTTAG, *β-actin-Rv*: CCCTGAAGTACCCCATTGAAC. Gene expression was normalized against endogenous control and $2^{-\delta\delta ct}$ values were calculated and presented as relative expression to naive cells. The eosinophil chemoattractant profile for lymphoid stromal cells were also analyzed using datasets available on Immgen.org. The data were presented as expression values normalized by DESeq2 without any modification.

Bulk RNA sequencing and analysis

Experiments were performed in triplicate wells and eosinophils were pooled post stimulation to create a single sample. RNA-seq was performed for duplicate samples per condition. Total RNA from eosinophils isolated from the co-culture was extracted using the Rneasy UCP Micro Kit (Qiagen) according to the manufacturer's instructions. cDNA libraries were constructed and sequenced by BGI Genomics (China) using DNBSEQ sequencing technology. Raw transcripts were filtered through SOA-Pnuke (V1.5.2) and hierarchical indexing for spliced alignment of transcripts 2 (HISAT2, V2.0.4) software was used to map the raw data reads. Raw data reads were mapped to the murine reference genome *Mus musculus*, NCIB: GCF_000001635.27_GRCm39. NOI-Seq analysis was used to identify differentially expressed genes (DEGs). DEGs were defined as log2 of the sample (expression value +1). Data were directly deposited to the BGI-Dr Tom web-based analysis portal. Read counts were normalized to FPKM (fragments per kilobase of transcript per million mapped reads). Gene set enrichment analysis (GSEA) was performed using normalized read counts, with a max threshold of 500 and a minimum threshold of 15 reads. GSEA enrichment plots were generated using the Kegg Pathway database. Phyper function in R was used to determine the P-value and the Q-value was obtained by correcting the false discovery rate (FRD) of the *p*-value. All data was analyzed and Reactome pathway enrichment was carried out using the BGI Dr. Tom system. All heatmaps, GSEA graphs, and enrichment plots were exported as.png files.

STRING analysis

Enriched genes from the bulk RNA seq were mined and analyzed using STRING platform V12 (https://cn.string-db.org/). The species was restricted to *Mus musculus*, and gene IDs derived from Dr. Tom were uploaded to the STRING platform. The STRING platform subnetwork analysis was performed on a given set of genes using GO term and biological processes annotation. The known interactions were shown using cyan and magenta lines and the predicted interactions were represented using green, red, blue, light green, and black lines. K-means clustering was also performed to find two defined clusters of proteins within the regulation of IL-5 production GO network, with each cluster highlighted using red or green color. The strength of the interaction is depicted by the line density based on predicted protein interactions from the String: protein query plug-in. The network maps were directly exported as a.png file. The gene set analysis datasets were exported to excel files and both counts within the network as well as the total network and background number were presented.

QUANTIFICATION AND STATISTICAL ANALYSIS

Statistical analysis

Image quantification was performed on serial sections as described earlier. Flow cytometry and gene expression analyses are expressed as means ± SEM. Statistical analyses were performed using a non-parametric Mann-Whitney Student's T test and ANOVA as indicated with post-hoc tests (Bonferroni's multiple comparison test). P-values indicated as $p < 0.05$ (*), $p < 0.01$ (**), $p < 0.001$ (***), $p < 0.0001$ (****). Graph generation and statistical analyses were performed using Prism version 10 software (Graph pad, La Jolla, CA).